RESEARCH PAPER P-506

REENTRY VEHICLE DISPERSION DUE TO ATMOSPHERIC VARIATIONS

Reinald G. Finke

August 1969

INSTITUTE FOR DEFENSE ANALYSES
SCIENCE AND TECHNOLOGY DIVISION

RESEARCH PAPER P-506

REENTRY VEHICLE DISPERSION DUE TO ATMOSPHERIC VARIATIONS

Reinald G. Finke

August 1969

INSTITUTE FOR DEFENSE ANALYSES
SCIENCE AND TECHNOLOGY DIVISION
400 Army-Navy Drive, Arlington, Virginia 22202

Contract DAHC15 67 C 0011
Task T-58

FOREWORD

The work reported in this paper was performed in support of the T-58 sub-task, Atmospheric Winds from Satellites, chaired by Dr. A.J. Grobecker. The text herein is extracted verbatim from Volume II: Potential Needs for Determination of Atmospheric Parameters of Study S-341 (Determination of Winds and Other Atmospheric Parameters by Satellite Techniques) by Dr. A.J. Grobecker, Mr. H. Hidalgo, Dr. R.G. Finke, and Dr. J.A. Laurmann in order to be disseminated to a separate distribution list of more specialized interest.

ACKNOWLEDGMENT

The author wishes to acknowledge the contributions of Dr. A.J. Grobecker and Mr. H. Hidalgo through many constructive discussions, and of Mr. E.T. Williams in arranging the machine calculations.

ABSTRACT

Reentry vehicle impact displacements due to a fixed perturbation in density or in wind speed in each 5-km-thick layer of the atmosphere up to 90-km altitude have been derived from a series of machine reentry-trajectory calculations with the IDA Program RANGE for different R/V's and reentry conditions. Three arbitrary reentry vehicle shapes were chosen whose ballistic coefficients (550, 1025, and 1975 lb/ft^2) were representative of the range of interesting values. Reentry conditions were varied, from those of IRBM's of 15,000 ft/sec at 50-deg path angle, to those for ICBM's of 22,500 ft/sec at 20-deg path angle, and reentry azimuths were varied from direct equatorial (tail wind) to retrograde equatorial (head wind). Intermediate reentry conditions were included to define the dependences well enough for interpolation, and even slight extrapolation, to all known interesting combinations.

The resulting layer-wise miss contributions from the most influential 5-km layers (centered at 5- and 10-km altitude) vary from about 200 ft for 1 percent change in density, or about 20 ft for 1 ft/sec change in wind speed for the low β and low reentry angle, to 0.4 ft for either 1 percent density change or 1 ft/sec of wind for the high β and high reentry angle.

At 60° N latitude, the worst-case, $\sim 2\sigma$ density and wind departures from a monthly mean profile occur in January and amount to about 5 percent in density and 50 ft/sec in wind in the most influential 5- to 10-km-altitude range. The corresponding total miss distances due to the combined departures from the mean profile for all altitudes range from several thousand feet for the low β, low reentry angle down to several tens of feet for the high β, high reentry angle. These total miss distances vary as the minus 1.5 to 2 power of β, as the minus 1 power

of reentry velocity, as the minus 3 to 5 power of the sine of the reentry angle, and negligibly with flight azimuth.

Allowable measurement errors for each layer to give a total impact uncertainty of 200 ft from combinations of all layers were derived. The minimum allowable errors in density and wind, occurring of course in the most influential 5- to 10-km layers, increase from the tightest extreme of about 0.1 percent and 1 ft/sec for low β, low reentry angle and combination as with common systematic error, to more than 50 percent and 200 ft/sec for high β, high reentry angle and combination as with random error.

CONTENTS

I. INTRODUCTION AND PRÉCIS

The atmosphere undergoes wide temporal variations in density and wind velocity, the two characteristics which most strongly influence the motion of an object such as a reentry vehicle passing through it. Diurnal or short-term meteorological fluctuations range from a few percent in density and ±30 ft/sec in wind at sea level, to extremes of ±25 percent in density and ±100 ft/sec in wind in the 100- to 200-kft altitude range. The short-term fluctuations are superimposed on seasonal variations which are of the same magnitude again, giving almost exactly double the variation when the two are concurrent.

The deceleration in g's of a reentry vehicle is given by the dynamic pressure ($q = 1/2\ \rho\ V^2$) divided by the ballistic coefficient ($\beta = W/C_D A$). The chief variations in the deceleration with altitude are in the exponential density ρ and the wind-velocity contribution to the relative velocity V in the dynamic pressure. For nonablative, nonpropulsive, nonmaneuvering R/V's, the weight W and reference area A do not change with altitude but the drag coefficient C_D has an altitude dependence through its Mach number dependence and the variation of Mach number with altitude. The shape of the R/V governs its drag coefficient and governs the dependence of the drag coefficient on Mach number and hence altitude. The existences of nonzero angle of attack, roll rate, and ablation introduce higher order altitude variations which depend intimately on initial conditions, mass distribution in the R/V, and aerodynamic normal force and moments.

The effect on the impact point of an R/V due to a change in density or wind velocity at some altitude is greater as the change is greater, as the density is greater, and as the time from that altitude to impact is greater. The latter two have opposite altitude dependences,

with time zero at maximum density and density zero at maximum time-to-impact, and lead to a maximum in influence at an intermediate altitude. A displacement in impact point can be considered to be the sum of miss contributions from different atmospheric layers, given by products of influence coefficients times changes in density or wind velocity for the respective altitude layers.

The variation with altitude of the influence coefficients depends also on the altitude variation of the deceleration. For a given change in atmospheric profile from a standard or mean profile, an impact displacement is generated which is different for different β's, reentry velocities, reentry angles, and flight azimuths.

A density or wind measurement uncertainty at a given altitude can be converted to a miss contribution by multiplying by the influence coefficient for that altitude. A maximum desired miss contribution can be converted to a maximum allowable measurement error by dividing by the influence factor. At that intermediate altitude where the largest influence factor occurs, the smallest allowable measurement error will apply, with the allowable error increasing at lower and higher altitudes.

II. VARIABILITY IN REENTRY ENVIRONMENT

A. ATMOSPHERIC PROFILES

For computation of actual reentry trajectories, specification of the atmospheric environment in more detail than that given by standard atmosphere tables requires knowledge of the temporal and geographical variation of the critical properties in each individual atmospheric layer. For the reentry vehicle, the time of launch and the places of launch and reentry must be specified to indicate from this information the most applicable reentry environment.

General trajectory calculations, giving extremes in variation of impact point, can be carried out for those dates and possible reentry locations which provide the widest variation in atmospheric profile. Figure 1 shows the departures in density profile between 0- and 90-km altitude for latitudes 15°, 30°, 45°, and 60° N latitude, for January and July, and for "cold" and "warm" days (CIRA, 1965). A representation of the diurnal density variability is given in Fig. 2 (U. S. Standard Atmosphere Supplement 1966). The "mean" profiles of January and July are essentially symmetrical on either side of the 1962 U. S. Standard Atmosphere over most of the altitude range, with January showing the greater spread from "cold" to "warm" days. The departures increase rapidly with latitude and, since 60° N is still within the range of interest, it was chosen as the reference latitude. The ends of the arrows on each side of the January mean profile represent approximately 95 percent departures (2σ if the weather variation followed a normal distribution); the mean January profile and the cold end of the arrows were taken as reference profiles. The diurnal variability was assumed to be included in the 2σ departures.

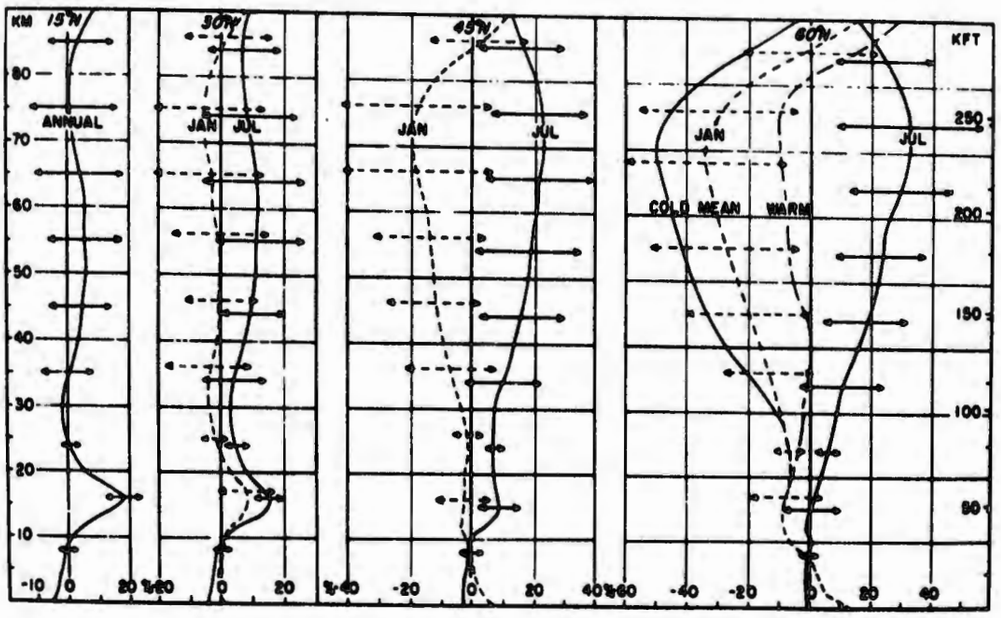

FIGURE 1. Seasonal Density Departures (in Percent) from the U.S. Standard Atmosphere 1962, for Four Latitudes (CIRA 1965)

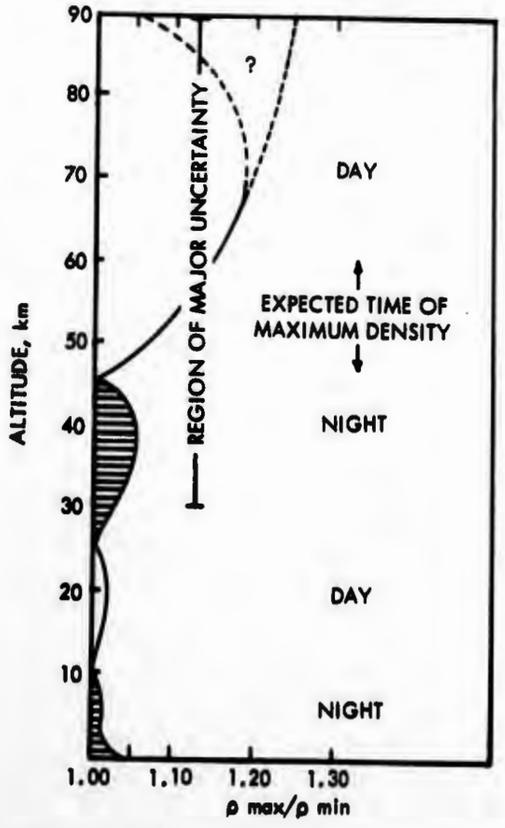

FIGURE 2. Approximate Values of Diurnal Density Variability up to 90 km (U.S. Standard Atmosphere Supplement 1966)

Wind-profile extremes for a fairly well investigated latitude, near 38° N, are reproduced in Fig. 3 (from Kochanski, 1964) to show the winter/summer symmetry about zero wind. A composite plot of data for prevailing westerly winter winds for latitudes 50° and 60° N and for altitudes of 0 to 30 km from Valley, 1965, and 30 to 90 km from U. S. Standard Atmosphere Supplement 1966, is given in Fig. 4. Up to about 40-km altitude, the "extreme" winter winds are almost exactly double the mean winter winds. "Extreme" is interpreted here as between 1 and 2σ in deviation from the mean; data are insufficient to define the deviation more accurately.

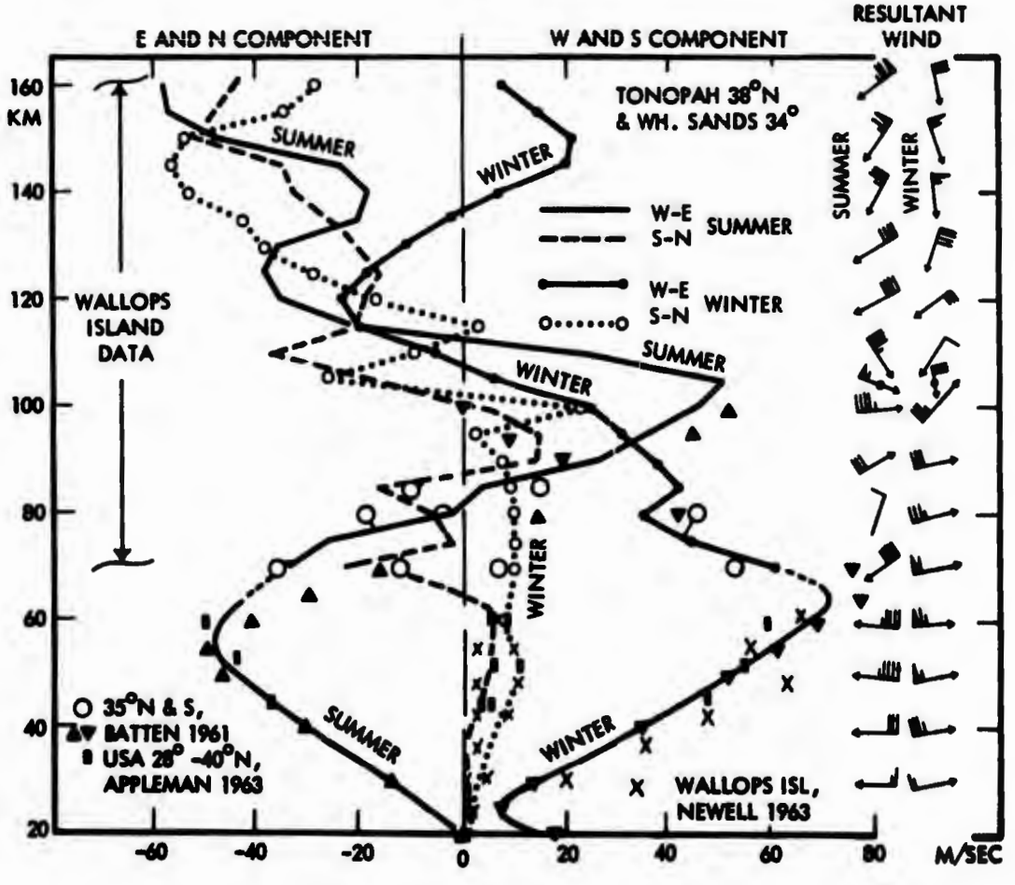

FIGURE 3. Wind Near 38° N (After Kochanski, 1964)

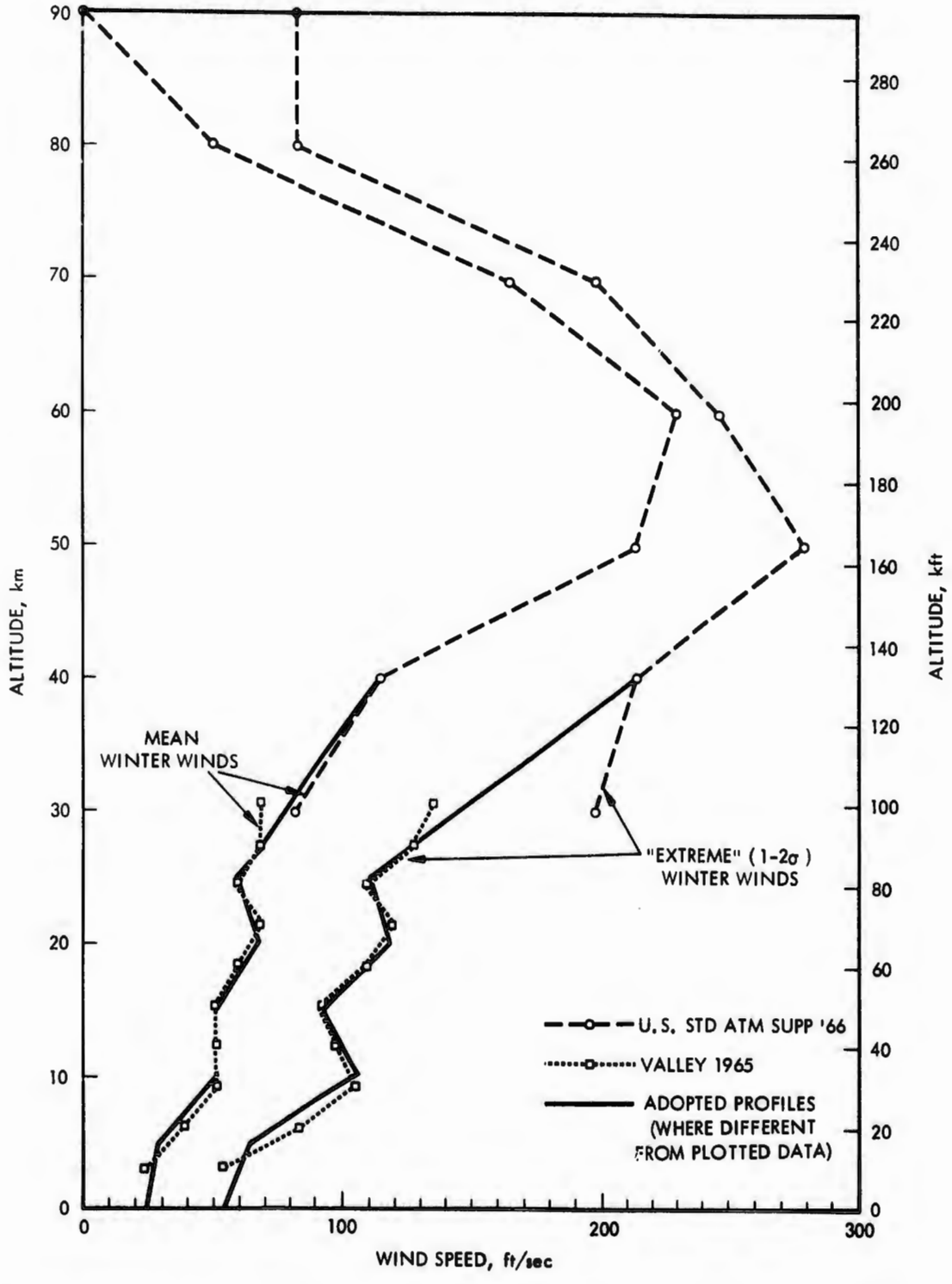

FIGURE 4. Composite Wind Speed Profiles for Winter 50° and 60° N Latitudes, West-to-East Direction

The curves in Figs. 1 and 4 have been converted to equivalent values at 5-km-altitude intervals for computer inputs and the values are listed in Table 1. Principal emphasis will be placed on the departure from the January mean density and the deviation from the mean winter wind in the ensuing evaluation of impact displacements.

TABLE 1. ADOPTED DENSITY AND WIND PROFILES FOR "COLDEST" DAY IN JANUARY AT 60° NORTH LATITUDE

Altitude		Density ($\Delta\rho/\rho$)		Wind Speed (Westerly)	
km	kft	January 2σ Departure from January Mean	January 2σ Departure from Annual Mean	Deviation (1-2σ) from Mean Winter Wind, ft/sec	Extreme (1-2σ) Winter Wind, ft/sec
0	0	+0.04	+0.13	30	54
5	16.4	+0.02	+0.03	35	64
10	32.8	-0.05	-0.12	54	105
15	49.2	-0.11	-0.20	42	93
20	65.6	-0.08	-0.13	51	118
25	82.0	-0.04	-0.11	51	110
30	98.4	-0.09	-0.20	66	144
35	114.8	-0.14	-0.27	83	179
40	131.2	-0.18	-0.33	98	213
45	147.6	-0.20	-0.40	82	245
50	164.0	-0.22	-0.46	66	279
55	180.4	-0.24	-0.50	41	262
60	196.8	-0.25	-0.54	16	246
65	213.3	-0.25	-0.57	24	221
70	229.7	-0.26	-0.59	33	197
75	246.1	-0.27	-0.57	33	140
80	262.5	-0.22	-0.45	33	82
85	278.9	-0.18	-0.35	57	82
90	295.3	-0.20	-0.31	82	82

B. DEPENDENCE OF $C_D(M,h)$ ON SHAPE OF REENTRY VEHICLE

The zero-lift drag coefficient for a reentry vehicle is synthesized in the RANGE trajectory program (Finke, 1963) from the shape of the vehicle, following closely the "simplified computer method" of NavWeps Report 1428. Four components are defined: (1) cone wave drag, (2) hemisphere wave drag, (3) base drag, and (4) skin-friction drag. A vehicle is described by the four corresponding factors: (1) cone half-angle in degrees, (2) ratio of hemispherical-nose cross-sectional area to cone base area, (3) fraction of cone base area contributing to base drag, and (4) ratio of skin surface area to cone base area.

Each component is a tabular function of Mach number and the fourth, skin friction, is also a function of ambient air density and hence altitude. The synthesized drag coefficient is, therefore, a complex function of Mach number and altitude which will be different in magnitude and form for different shape reentry vehicles.

The ballistic coefficient of a reentry vehicle is in effect defined using the hypersonic inviscid drag coefficient, i.e., that for velocities above about Mach 10 where the base drag coefficient has diminished to negligible values and for altitudes below about 200 kft where the skin-friction drag coefficient has diminished to negligible values. At lower Mach numbers and at higher altitudes, the C_D generally increases above and the β decreases below the reference value.

Three different reentry vehicles characteristic of principal existing classes were selected for this study. Their descriptive parameters are given in Table 2 and scaled shapes in Fig. 5. The weight and reference area were chosen to make C_DA equal to 1 ft^2 in the hypersonic inviscid flight regime. This arbitrary area assumption affects the scale of the vehicle only, influencing the Reynolds number and hence the altitude for transition to turbulent flow. The contribution due to skin-friction drag is so small, a few percent (see below) in the likely range of transition altitudes, that a change in transition altitude by a scale height, a factor of e^2 in area and weight, would have negligible influence on the impact point.

β = 550 LB/FT^2; W = 550 LB

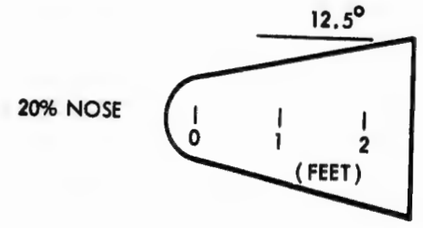

β = 1025 LB/FT^2; W = 1025 LB

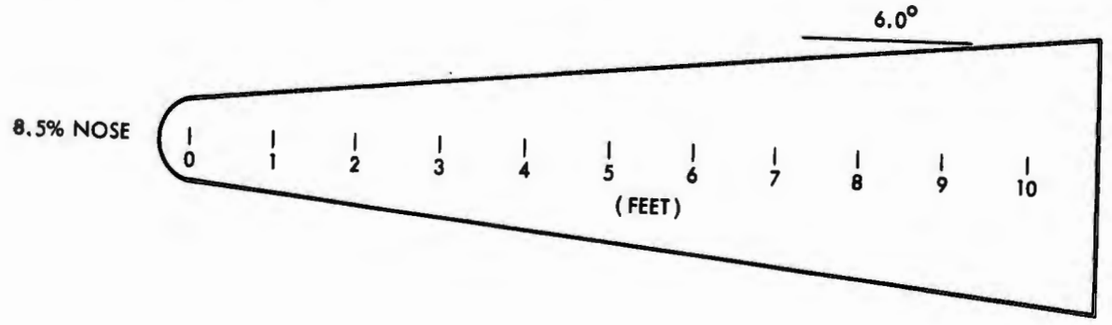

β = 1975 LB/FT^2; W = 1975 LB

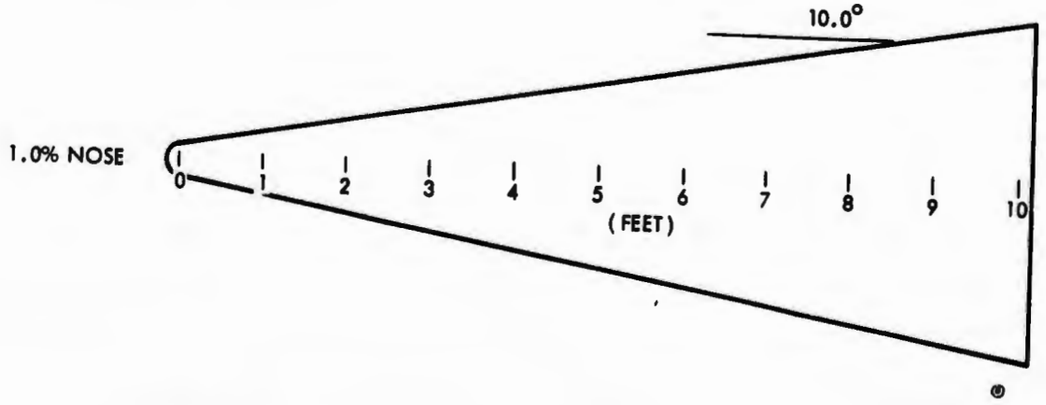

FIGURE 5. Scaled Arbitrary Reentry Vehicle Configurations

TABLE 2. SELECTED REENTRY VEHICLES

β, lb/ft^2	W, lb	A, ft^2	Cone Angle, deg	Nose Ratio	Base Ratio	Skin Ratio
550	550	3.234	12.5	0.20	1.00	4.62
1025	1025	8.149	6.0	0.085	1.00	9.58
1975	1975	12.438	10.0	0.01	1.00	5.76

Plots of C_DA versus Mach number (with altitude implicit) and versus altitude (with Mach number implicit) are shown for the three vehicles in Figs. 6 and 7 for zero-angle-of-attack reentry trajectories starting at 400-kft altitude at -20 deg path angle and 22,500 ft/sec velocity from a direct equatorial (tail-wind) flight path. The Mach number/altitude plots are given in Fig. 8. The low-Mach-number values of C_DA increase as the relative contribution of hemisphere drag (nose ratio) decreases and cone drag becomes paramount, and the high-altitude values increase with the relative contribution of skin friction (skin surface area ratio). The tiny loop on the curves in Fig. 6 near Mach 22 represents transition to turbulent flow and the reversal in direction of the curves at Mach 21 is a consequence of the reversal in lapse rate at 155-kft altitude in the 1962 atmosphere, from zero and negative above that altitude to positive below. Similar behavior occurs at Mach 25.6. The transition to turbulent flow is barely noticeable at the marks in Fig. 7 at about 85- to 100-kft (25- to 30-km) altitude. Passage through the transonic drag peak occurs at higher altitudes for lower β, overriding all other low-altitude effects.

C. UNCERTAINTIES IN ANGLE OF ATTACK, ROLL RATE, AND ABLATION

The three-degree-of-freedom RANGE program is capable of calculation of trajectories of point-mass vehicles with arbitrarily specified angles of attack and roll. Flight behavior of a distributed-mass vehicle, with its accompanying moments of inertia and aerodynamic moments, requires calculation with a six-degree-of-freedom program. Use of the APL six-degree-of-freedom program, FLIGHT (Albini and Glover, 1966), to its full capability involves an increase in computing time by a factor of 25 to

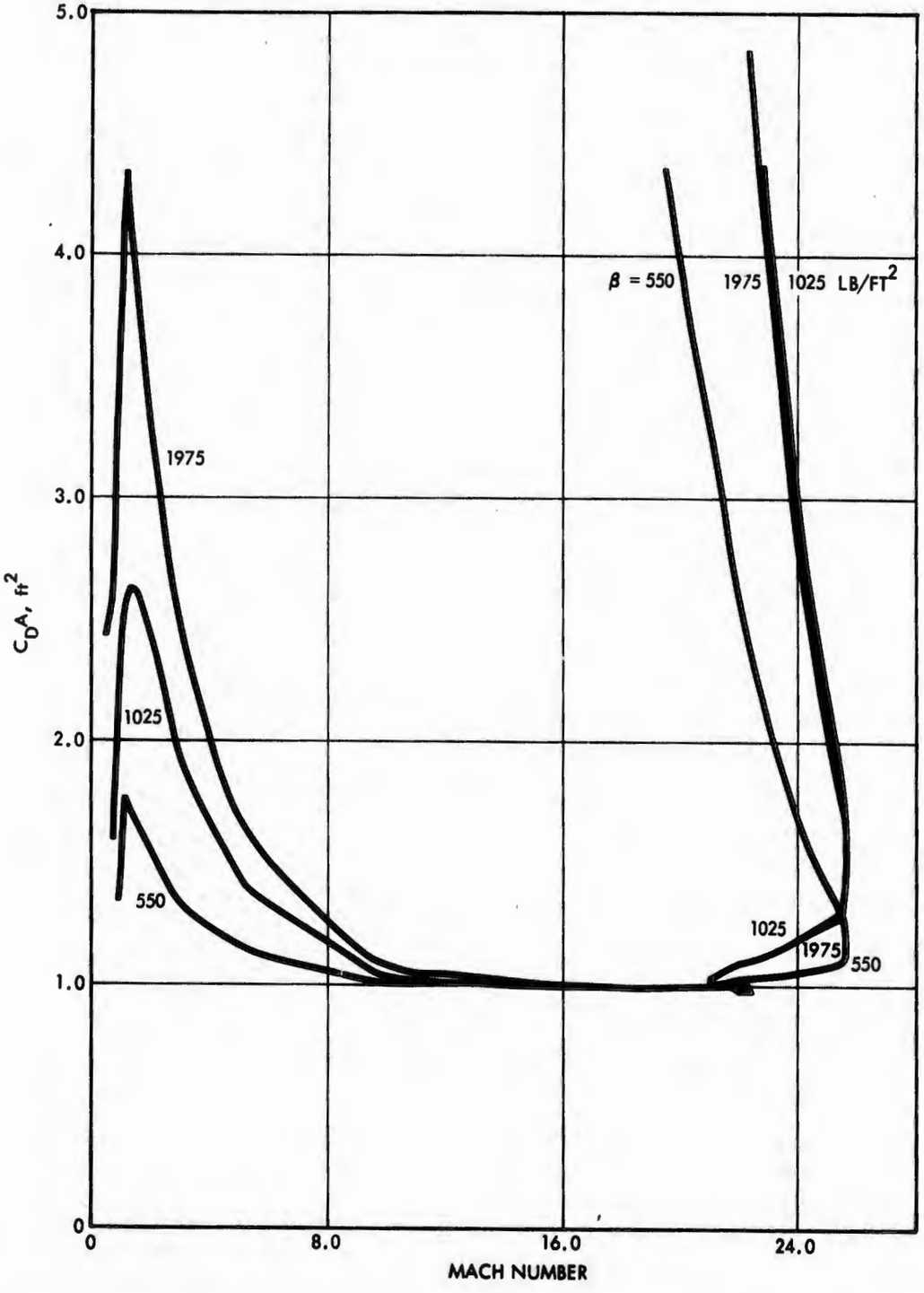

FIGURE 6. Mach Number Dependence of Drag Coefficients of Three Different Reentry Vehicles with β's of 550, 1025, and 1975 lb/ft^2, for Reentry Trajectories with 22,500 ft/sec Reentry Velocity and -20 Deg Path Angle. Weight and Reference Area are Chosen to Make C_DA Equal to 1 ft^2 in the Hypersonic Inviscid Regime.

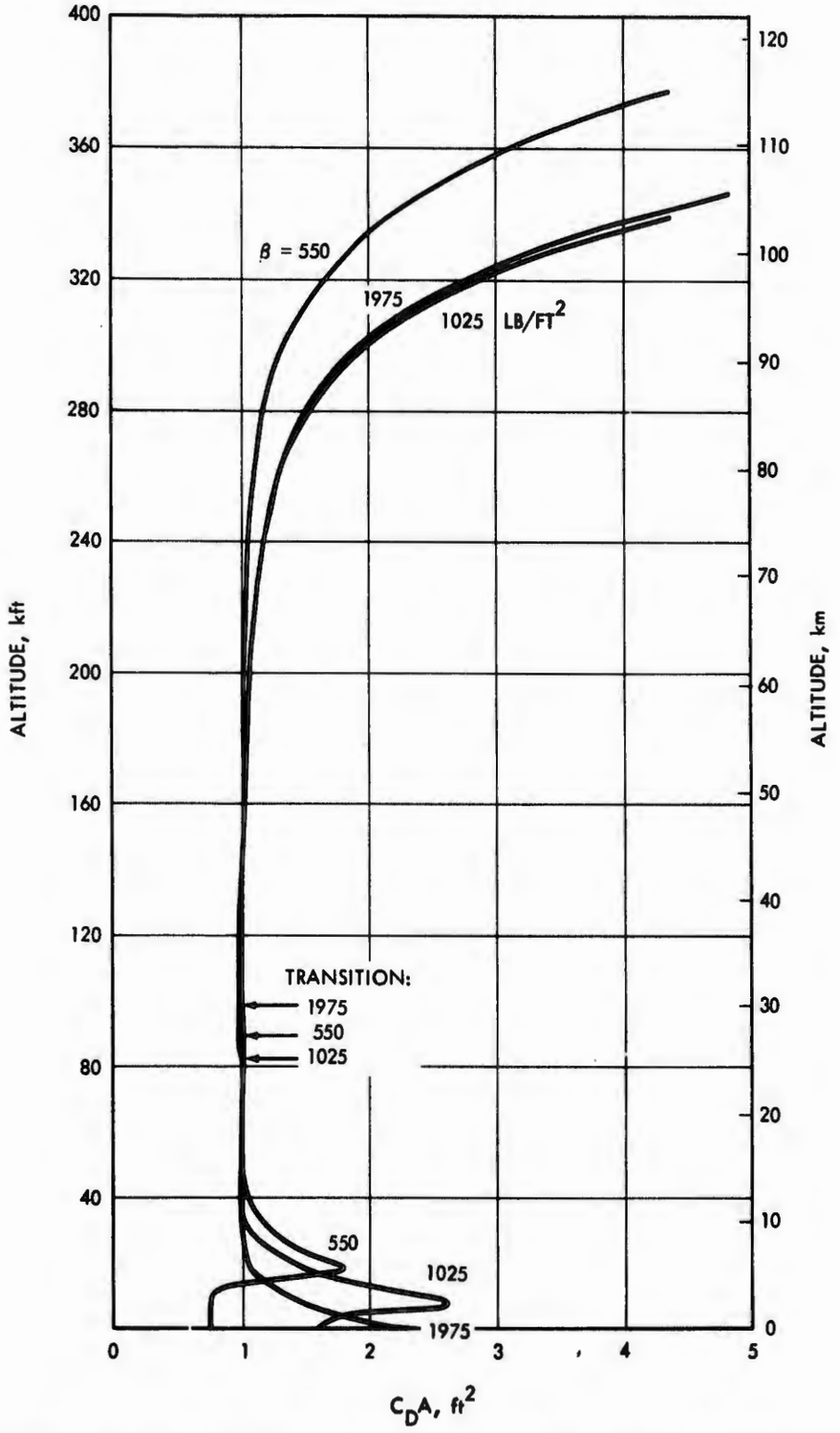

FIGURE 7. Altitude Dependence of Drag Coefficients of Three Different Reentry Vehicles with β's of 550, 1025, and 1975 lb/ft^2 for Reentry Trajectories with 22,500 ft/sec Reentry Velocity and -20 deg Path Angle. Weight and Reference Area are Chosen to Make C_DA Equal to 1 ft^2 in the Hypersonic Inviscid Engine.

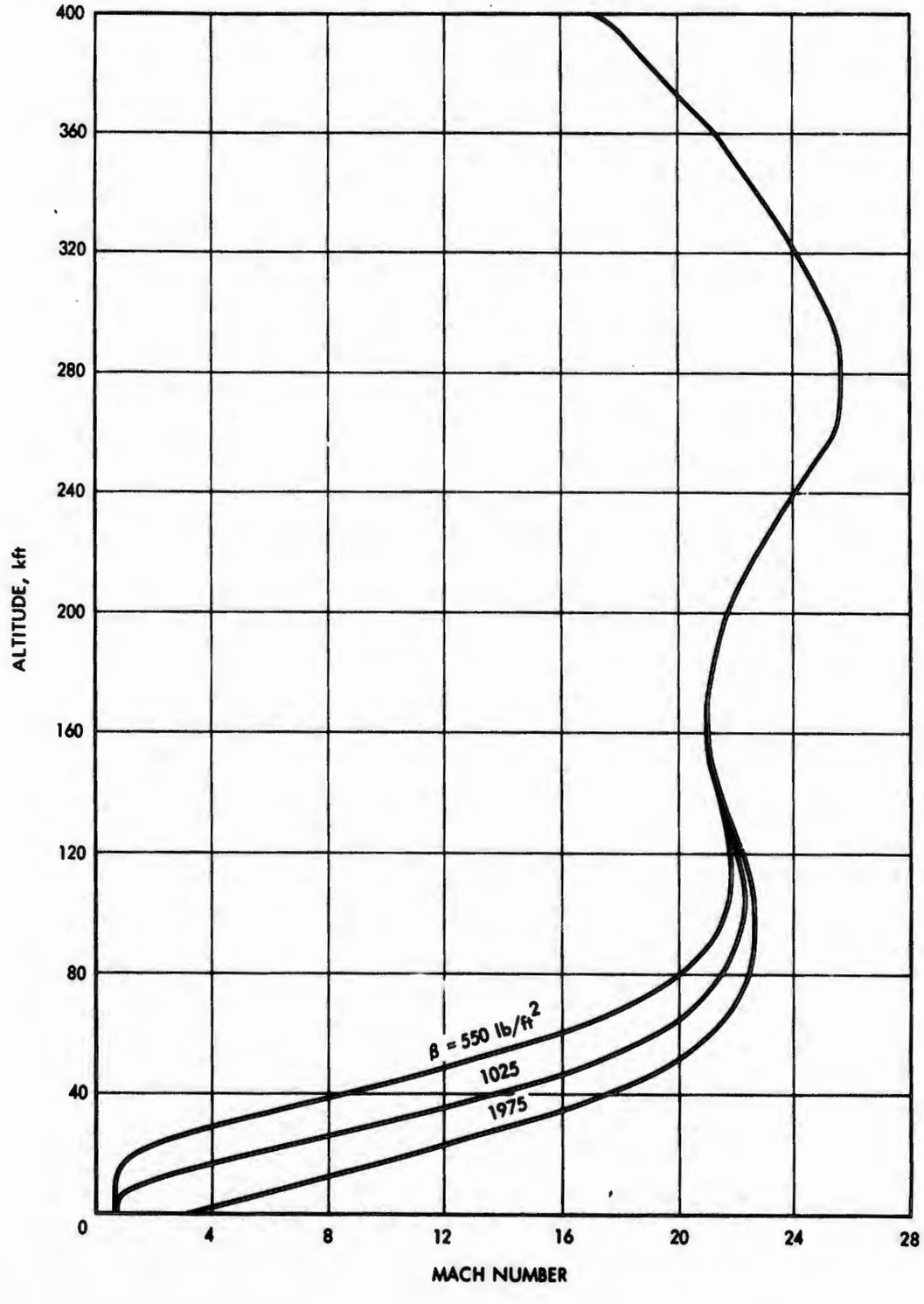

FIGURE 8. Altitude/Mach Number Plot for Three Different Reentry Vehicles with β's of 550, 1025, and 1975 lb/ft^2 for Reentry Trajectories with 22,500 ft/sec Reentry Velocity and -20 deg Path Angle

50 over RANGE, i.e., 20 to 35 min for ballistic reentry problems taking 40 to 50 sec with RANGE.

The comparative simulation capabilities of three degrees of freedom versus six degrees of freedom were examined by running a series of test problems with the FLIGHT (6-deg) program. First, differences in axial force coefficient between the two programs were reduced to less than 0.5 percent at altitudes between 5 and 200 kft by adjusting the FLIGHT program drag-factor inputs. Second, the roll rate was set to zero to eliminate the greatest difference between the two simulations, giving an impact point essentially identical (within 1 ft) of the RANGE value. Introducing an initial angle of attack of 20 deg to measure the longitudinal effects of the mass distribution gave a difference in impact point of less than 10 ft. A roll rate of 360 deg/sec (with zero initial angle of attack) moved the impact point also by less than 10 ft. Combining a 20-deg initial angle of attack and the roll rate gave an impact displacement of 120 ft. A similar run with the initial 20 deg in yaw rather than pitch gave a displacement of 280 ft. So, for nominally zero initial attitude angles, the difference between six-degree and three-degree-of-freedom simulations is negligible. For specific initial attitude angles, however, and also probably for a change in figure and a center-of-gravity offset associated with non-uniform ablation, the six-degree-of-freedom program is essential. These off-nominal conditions are not specified for this general analysis so no advantage could be gained in using the six-degree-of-freedom program that would outweigh its increase in computing time.

A final test of the six-degree-of-freedom program with a change in atmospheric density profile from the January mean to the January 2σ departure, for the β = 1975 lb/ft^2, γ_o = 20 deg, V_o = 22,500 ft/sec, 360-deg/sec-roll-rate case, gave an impact displacement of 351 ft versus the RANGE (3-deg) value of 370 ft.

III. RELATIVE INFLUENCE OF DIFFERENT ATMOSPHERIC LAYERS

A. ANALYTIC ESTIMATE FOR CROSS WIND

Of ultimate importance in this paper is, of course, the numerical evaluation of the influence of wind and density departures in different atmospheric layers on the impact displacement of a reentry vehicle. However, a derivation of the functional dependences of these influence coefficients on the atmospheric and vehicle parameters for a simplified case is useful to provide a feel for the effects of the different parameters. The normally complex altitude dependences of atmospheric density, drag coefficient, velocity, and path angle require solution in general by numerical integration of the equations of motion, and an analytic estimate can be made only for a special case.

The following simplifications are invoked to improve the tractability of the problem:

1. The atmospheric departure is a small cross wind only (the effective change of drag vector is in direction only and not magnitude).
2. The reentry vehicle has a high, constant β (altitude dependences of velocity and β are small enough to be neglected).
3. The reentry vehicle is a point mass with no angle of attack (normal forces, moments, and transient response are ignored).
4. The force of gravity is negligible with respect to the drag force (change in path angle is ignored).
5. The atmospheric density is a simple exponential function of altitude (allows use of an analytic expression).

The vector diagram of the velocities and forces, given in Fig. 9, is viewed from a direction perpendicular to both the wind velocity vector, w, and the reentry vehicle's velocity vector relative to the earth's surface, V_e.

FIGURE 9. Velocity and Force Vectors

The drag D is parallel and opposite in sign to the velocity relative to the air, V, rather than V_e, so there is generated in effect a lateral force, F, perpendicular to V_e given by

$$F = \frac{Dw}{V} \tag{1}$$

The acceleration produced by a force acting on a mass W over a time interval δt gives a velocity increment

$$\delta V = a\delta t = \frac{Dw\delta t}{WV} \tag{2}$$

where the time δt to pass through a given atmospheric layer of thickness δh with a path angle γ from the horizontal is

$$\delta t = \frac{\delta h}{V\sin\gamma} \tag{3}$$

The time-to-impact, t, from the altitude h is given approximately by

$$t \approx \frac{h}{V\sin\gamma} \tag{4}$$

The lateral impact displacement δy due to the altitude layer δh is the product of the velocity increment δV times the time-to-impact t, or

$$\delta y = t\delta V$$

$$= \frac{Dwh\delta h}{WV^3 \sin^2\gamma} \tag{5}$$

Substituting the expressions for drag

$$D = C_D A \tfrac{1}{2} \rho V^2 \tag{6}$$

and the exponential atmosphere

$$\rho = \rho_o e^{-h/S} \tag{7}$$

into Eq. 5 gives

$$\delta y = \frac{\frac{1}{2}\rho_o}{\beta} \frac{w}{V\sin^2\gamma} he^{-h/S}\delta h \tag{8}$$

The atmospheric and vehicle constants are

$\rho_o = 0.0765$ lb/ft^3 = atmospheric density at sea level

$S \approx 23{,}000$ ft = scale height (e-folding altitude increment) of atmosphere

$\beta = W/C_D A$ = ballistic coefficient

For a division of the atmosphere into layers of one scale height thickness with a different value of the cross wind velocity w_n in each layer, expression (8) can be integrated over the n^{th} layer to produce the miss contribution Δy_{nw} from that layer:

$$\Delta y_{nw} = \tfrac{1}{2} \frac{\rho_o w_n}{\beta V_n \sin^2 \gamma_n} \int_{(n-1)S}^{nS} h e^{-h/S} dh \qquad (9)$$

$$= \tfrac{1}{2} \frac{\rho_o w_n S^2}{\beta V_n \sin^2 \gamma_n} e^{-n\left[n(e-1)-1\right]} \qquad (10)$$

This first-order approximation indicates that the miss contribution will decrease as the ballistic coefficient, reentry velocity, and reentry path angle increase, and will be proportional, as expected, to the wind speed.

Values for the exponential term $K_n = e^{-n\left[n(e-1)-1\right]}$ are listed in Table 3. The highest value is in the second scale height layer, illustrating the crossover from the opposite altitude dependences of the two governing variables, ambient density, and time-to-impact.

TABLE 3. APPROXIMATE RELATIVE INFLUENCE OF DIFFERENT SCALE HEIGHT LAYERS FROM EXPONENTIAL EXPRESSION IN EQUATION 10: $K_n = e^{-n\left[n(e-1)-1\right]}$. SCALE HEIGHT TAKEN AS 23,000 FT

Layer, Scale Heights	Altitude Range, kft	K_n	$\sum_{i=n+1}^{\infty} K_i$	U.S. Std Atmos 1962 e-Folding Altitudes, kft
1	0 to 23	0.2643	0.7357	(30.5)
2	46	0.3296	0.4061	(52.6)
3	69	0.2068	0.1993	(73.3)
4	92	0.1076	0.0917	(94.2)
5	115	0.0512	0.0405	(115.4)
6	138	0.0231	0.0174	(137.5)
7	161	0.0101	0.0073	(161.8)
8	184	0.0043	0.0030	(188.9)
9	207	0.0018	0.0012	(215.9)
10	207 to 230	0.0007	0.0005	(240.4)

An interesting sidelight stems from the fact that

$$\sum_{n=1}^{\infty} K_n = 1 \tag{11}$$

which implies that, for a wind speed profile that is a constant independent of altitude, the total impact displacement ΔR in the lateral (y) direction due to wind (w) can be expressed as

$$\Delta R_{yw} = \tfrac{1}{2} \frac{\rho_o w S^2}{\beta V \sin^2 \gamma} \tag{12}$$

While Eq. 12 applies only to an idealized wind profile, it provides a simple analytical expression that can be readily evaluated for comparison with results obtained more accurately with machine trajectory calculations with the same profile. For values of the parameters

$w = 100$ ft/sec

$\beta = 1975$ lb/ft^2

$V = 22{,}500$ ft/sec

$\gamma = 20$ deg

the total impact displacement from Eq. 12 is 390 ft. This is to be compared with 760 ft obtained by trajectory calculations with the RANGE program with the constant wind profile but with the proper altitude dependence of all other properties. When the n^{th} scale height's contribution is corrected by using in Eq. 10 the average velocity V_n in the layer, computed by RANGE, the estimate of total impact displacement is improved from 390 ft to 620 ft, which is a reasonable approximation to the result from detailed trajectory calculations.

Given also in Table 3 is $\sum_{i=n+1}^{\infty} K_i$, the summation of the contributions from all other layers above the n^{th}. For a wind profile with constant values, this expression gives the error in estimating the impact displacement due to neglecting the contributions from higher altitudes than the n^{th}. For example, in this simplified case, neglecting the effects of a constant wind above 70 kft would ignore about 20

percent of the impact displacement, and above 90 kft about 10 percent. Since the wind speed is generally higher above these altitudes than below (Fig. 4 and Table 1), the errors would be correspondingly higher.

We can define an "influence coefficient" from Eq. 10 approximately as

$$B_n = \tfrac{1}{2} \frac{\rho_o S^2 K_n}{\beta_n V_n \sin^2 \gamma_n} \quad (13)$$

so that the total impact displacement can be expressed in terms of any wind profile $w_n = f(n)$ as

$$\Delta R_{yw} = \sum_{n=1}^{\infty} B_n w_n \quad (14)$$

B. INFLUENCE COEFFICIENTS FROM MACHINE CALCULATIONS

The influence coefficient for a departure from a standard condition in a given atmospheric layer can be defined as the impact displacement resulting from a unit change in the atmospheric characteristic in that layer, e.g., from a 1 ft/sec change in wind velocity or a 1 percent change in density. The tables of departures (Table 1) from standard wind and density profiles are listed for machine input at nineteen 5-km (16,404 ft) levels from 0 to 90 km, with a slight incidental improvement in resolution over the ten layers of Table 3. Introducing a fixed perturbation into each one of these entries respectively, and performing a series of otherwise identical machine reentry-trajectory calculations, generates a series of impact displacements that represents the influence coefficients for the set of 5-km-altitude levels for a given reentry vehicle and given initial conditions. (In this treatment, a perturbation in the tabular entry at the 5-km level, for instance, is equivalent to a perturbation in the 2.5- to 7.5-km layer, not the 0- to 5-km layer as before.)

Perturbations of 500 ft/sec in wind velocity and 50 percent in density were chosen to provide miss contributions that were large enough from all the altitudes to be significant in comparison with

finite-integration-step and round-off errors in the machine calculation. However, these perturbations are, first, larger than actual wind and density variations, raising a question of linearity of the effects over this wide a range; and, second, made one level at a time, raising a question about interaction between layers when layer-wise effects are added linearly to represent the effects of a profile.

The closeness to linearity of the effects of a series of increasing perturbations at one level is shown in Fig. 10 for a high-influence level (5 km) and for values of β (550 lb/ft^2), reentry angle (-20 deg), and reentry velocity (22,500 ft/sec) which give large effects. The largest departure from linearity in the middle of the range for wind is only about 1.5 percent of the full 500 ft/sec impact displacement but for density amounts to about 7 percent of the full 50 percent density effect.

As a more realistic test of the combined effects of interaction between the levels and the nonlinearity of the miss contributions for these large perturbations, the sum of the miss contributions from the individual perturbations was compared with the impact displacement for nominal reentries having the perturbations incorporated in all levels at the same time. The sum exceeded the integral by only about 0.5 percent for the 500 ft/sec wind perturbation but by about 25 percent for the 50 percent density perturbation. Further comparisons of 2/5 of the sum of the 50 percent density miss contributions against the impact displacement from simultaneous incorporation at all altitudes of 2/5 of the perturbation (20 percent in density) gave agreement within 5 percent, less than one-third of the error attributable to nonlinearity alone. The worst density departures (Table 1) are 20 percent or less in the more important layers, below 100 kft, where about 90 percent (Table 3) of the impact displacement is generated.

The influence coefficients, that is, the miss contributions for the 500 ft/sec wind and 50 percent density perturbations in 5-km layers, for the levels from 0 to 90 km have been calculated with the RANGE program for 27 indicative combinations of the following parameters:

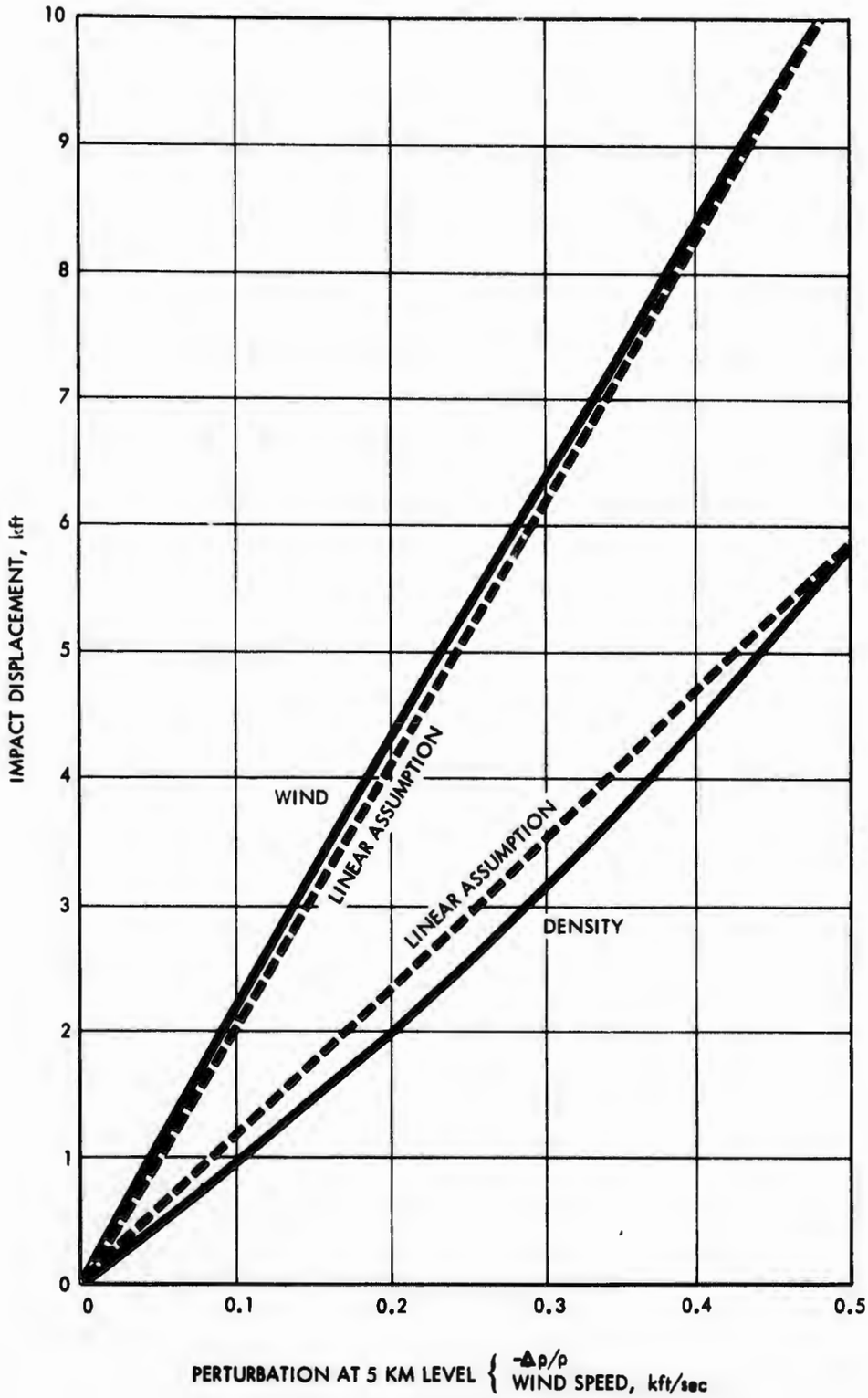

FIGURE 10. Departure from Linearity of Impact Displacement for Different Wind and Density Perturbations at 5-km level ($\beta = 550$ lb/ft^2; $\gamma_o = 20°$; $V_o = 22{,}500$ ft/sec)

- The three reentry vehicles in Table 2 (β's of 550, 1025, and 1975 lb/ft^2);
- Reentry velocities of 22,500, 18,750, and 15,000 ft/sec;
- Reentry angles of 20, 30, 40, and 50 deg; and
- Equivalent orbital inclinations of 1, 89, and 179 deg (tail wind, cross wind, and head wind).

Plots of the resulting miss contributions versus altitude are given in Fig. 11 for the three β's, for the set of reentry angles, and for the 22,500 ft/sec and 15,000 ft/sec reentry velocities. The velocity dependence (e.g., from comparison of the 22,500 ft/sec and 15,000 ft/sec curves for the same reentry angle) is so small and so linear that the 18,750-ft/sec curves were not included. Similarly, the dependence on orbital inclination is so small (see later discussion) that the curves for inclinations other than 1 deg were not included.

The trends in the plots in Fig. 11 show the increasing miss contributions with decreasing β, reentry angle, and velocity, and show the more rapid variation of density effects than wind effects with these parameters, with a shift towards predominance of wind effects at higher β's and higher reentry angles.

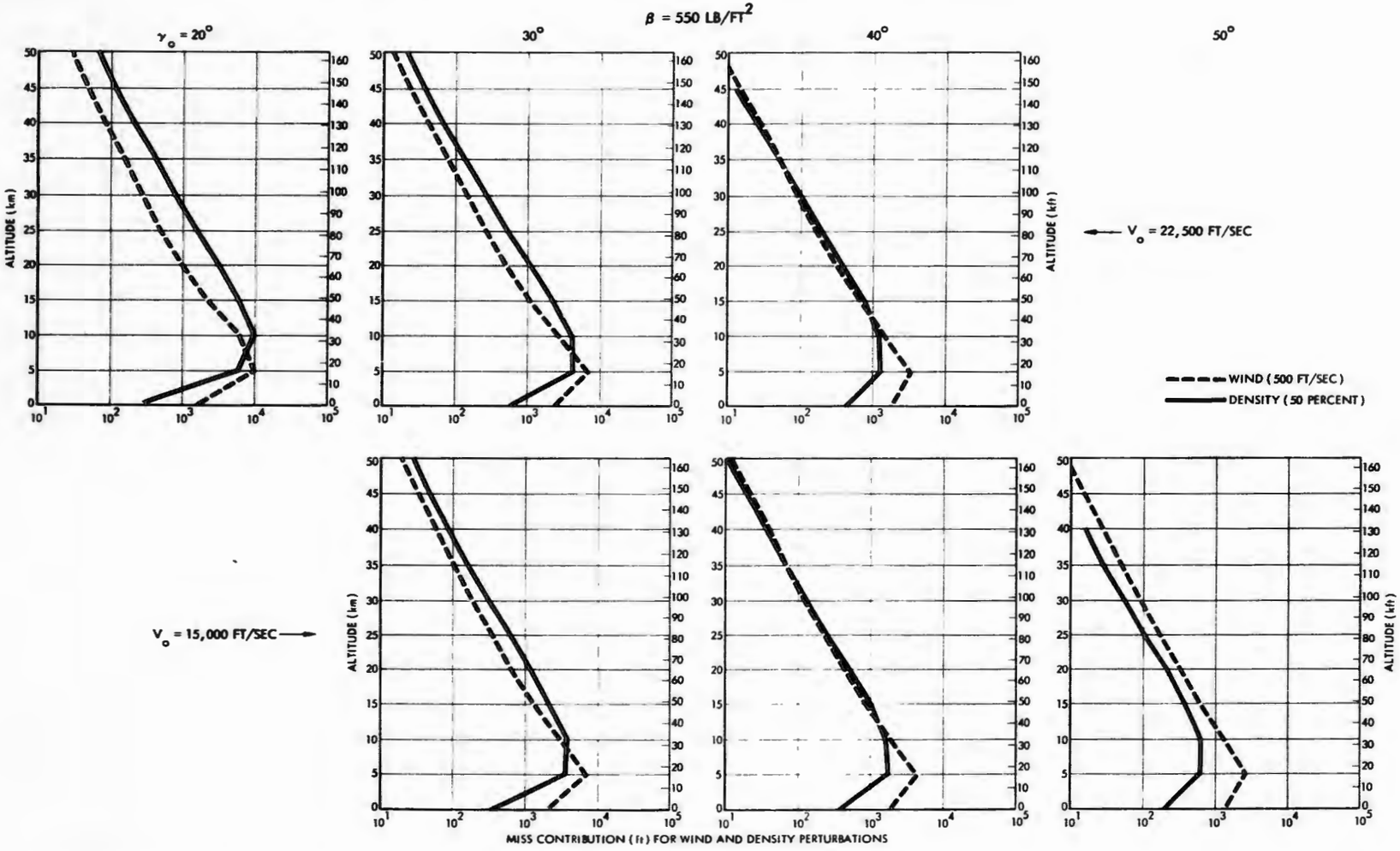

FIGURE 11a. Miss Contribution of Each 5 km Layer for Perturbations in Wind of 500 ft/sec and Density of 50 Percent. Reentry Vehicle with W/C_DA of 550 lb/ft^2 and with Different Reentry Angles and Reentry Velocities.

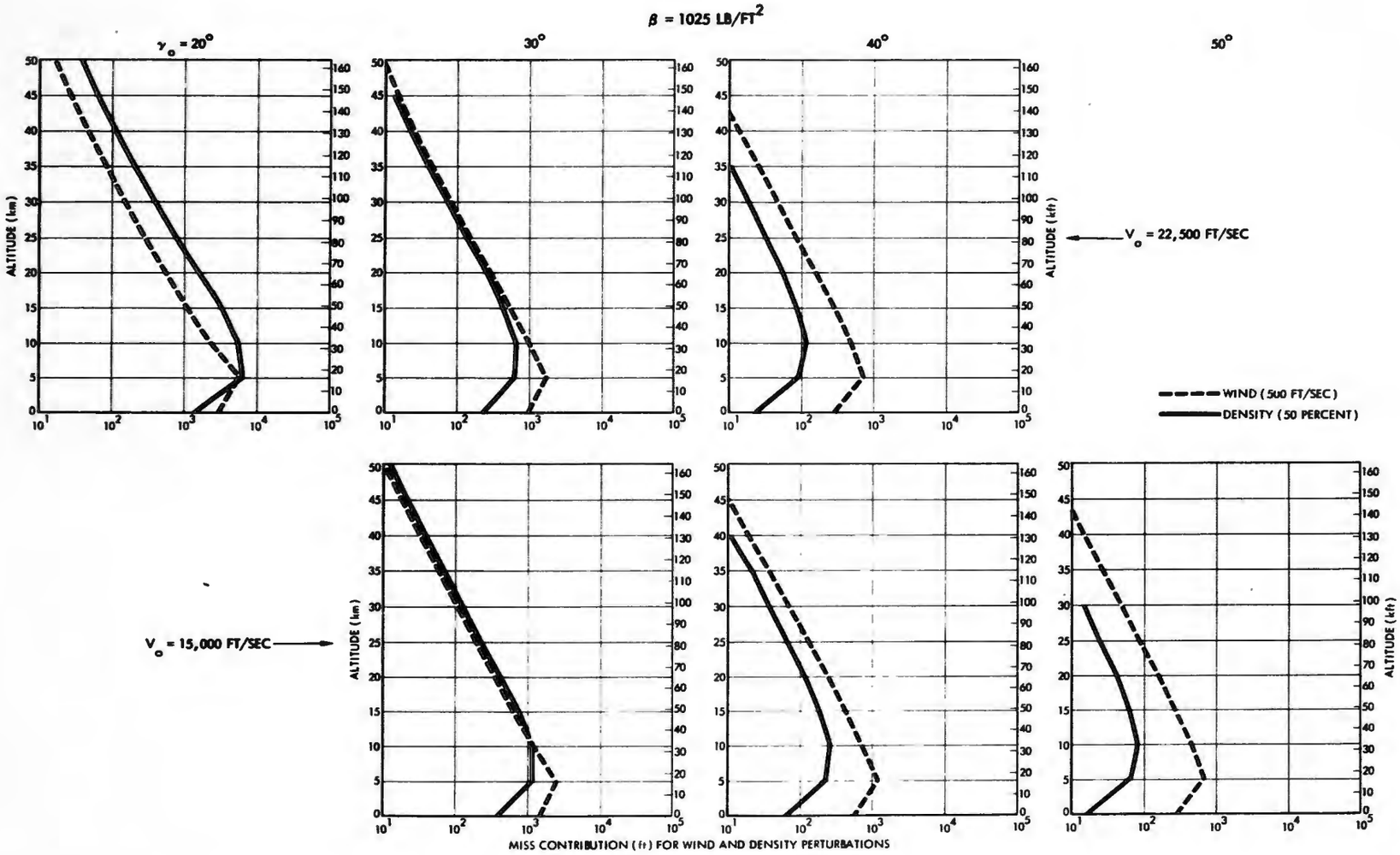

FIGURE 11b. Miss Contribution of Each 5 km Layer for Perturbations in Wind of 500 ft/sec and Density of 50 Percent. Reentry Vehicle with W/C_DA of 1025 lb/ft^2 and with Different Reentry Angles and Reentry Velocities.

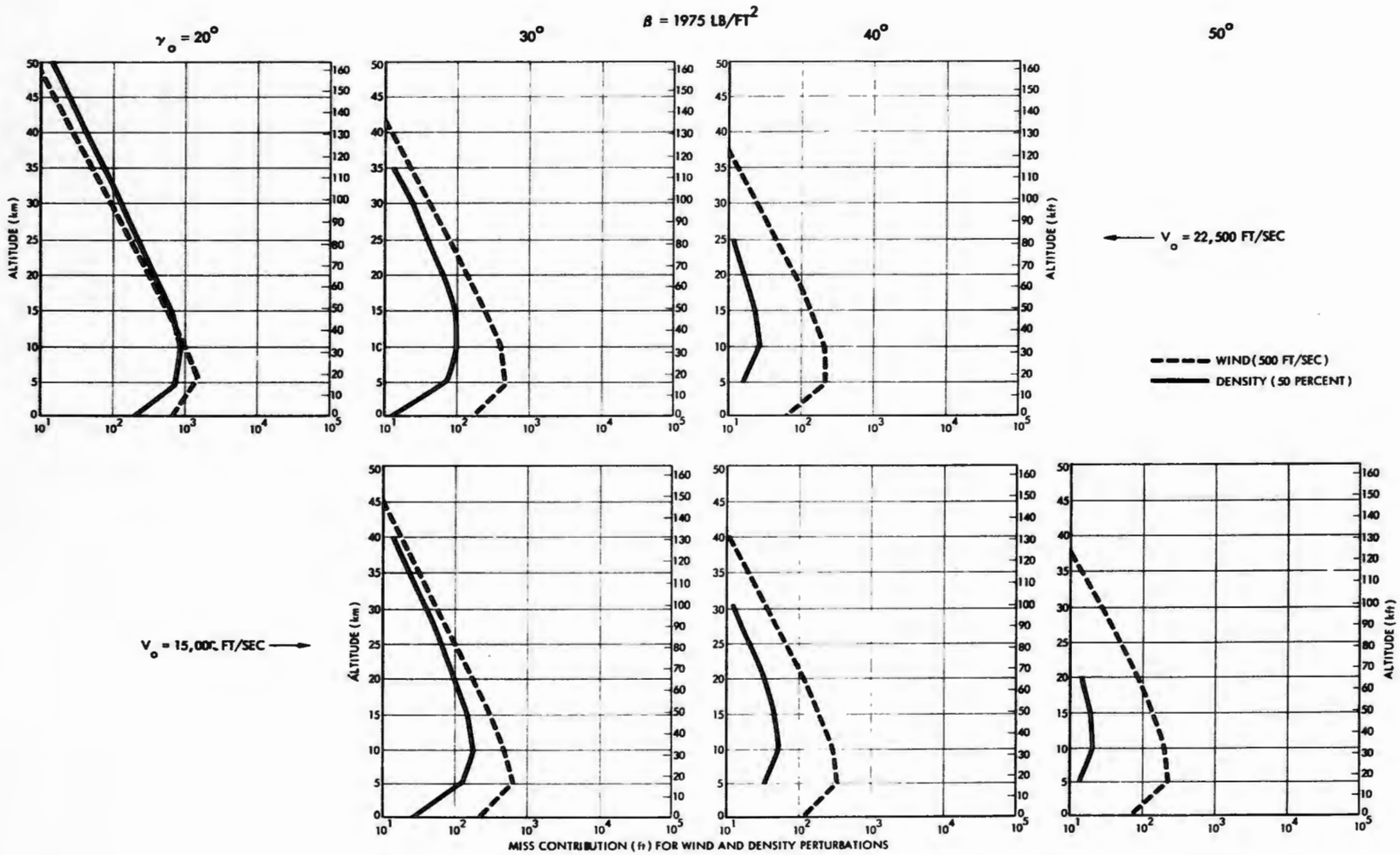

FIGURE 11c. Miss Contribution of Each 5 km Layer for Perturbations in Wind of 500 ft/sec and Density of 50 Percent. Reentry Vehicle with W/C_DA of 1975 lb/ft^2 and with Different Reentry Angles and Reentry Velocities.

IV. PARAMETRIC DEPENDENCES OF MISS DISTANCES FOR ATMOSPHERIC PROFILE DEPARTURES

A. CALCULATION OF MISS DISTANCES

The influence coefficients generated by the series of reentry trajectory calculations exhibit marked dependences on the reentry parameters, as can be seen by detailed comparisons of the curves in Fig. 11. A more readily interpretable display of these dependences can be arranged by applying the influence coefficients to reference profiles of wind and density departures to obtain the associated miss distances, ΔR, through the linearized relations (cf. Eq. 14):

$$\Delta R_{x\rho} = \sum_{i=1}^{19} \Delta x_{i\rho} \left.\frac{\Delta\rho}{\rho}\right|_i / 0.5 \tag{15a}$$

$$\Delta R_{y\rho} = \sum_{i=1}^{19} \Delta y_{i\rho} \left.\frac{\Delta\rho}{\rho}\right|_i / 0.5 \tag{15b}$$

$$\Delta R_{xw} = \sum_{i=1}^{19} \Delta x_{iw} \, w_i / 500 \tag{15c}$$

$$\Delta R_{yw} = \sum_{i=1}^{19} \Delta y_{iw} \, w_i / 500, \tag{15d}$$

The $\frac{\Delta\rho}{\rho}\Big|_i$ and w_i are density and wind departures from the 1962 Standard Atmosphere for the nineteen 5-km-interval levels from 0- to 90-km altitude, and the $\Delta x_{i\rho}$, Δx_{iw} and $\Delta y_{i\rho}$, Δy_{iw} are, respectively, the density and wind influence coefficients (miss contributions from Fig. 11) in the downrange and crossrange directions resulting from a 50 percent density perturbation or a 500 ft/sec wind velocity perturbation at the i^{th} altitude level. The crossrange miss distances ΔR_y are negligible with respect to (less than a few percent of) the downrange miss distances ΔR_x for all the chosen values of the reentry parameters except the case of a cross wind (i_o = 89 deg). The values of the reentry parameters selected for machine calculation were the following. For each of the three β's (i.e., 550, 1025, and 1975 lb/ft^2), nine combinations of reentry velocity (V_o), reentry angle (γ_o), and equivalent orbital inclination (i_o) were taken to provide at least one cross section in each dimension:

V_o ft/sec	γ_o deg	i_o deg
22,500	20	179 (head wind)
22,500	20	89 (cross wind)
22,500	20	1 (tail wind)
22,500	30	1
22,500	40	1
18,750	30	1
15,000	30	1
15,000	40	1
15,000	50	1

With a set of 39 problems (i.e., a basic unperturbed problem, 19 density perturbations, and 19 wind perturbations), for each of the 27 combinations above, this parameter study comprised 1053 individual reentry trajectory calculations.

Each of the 27 sets (times two; one each for density and wind) of influence coefficients was applied through Eqs. 15 to the density and wind profiles given in Table 1, generating sets of $\Delta R_{x\rho}$ and ΔR_{xw} (or ΔR_{yw} for the i_o = 89 deg case) from which the influences of β, V_o, γ_o, and i_o on miss distance could be easily plotted. A summary of the miss distances for all the cases for the density and wind profiles representing the maximum January departure from the January mean is given in Table 4. The miss distances for the maximum January departure from the annual mean are not tabulated because they are almost exactly (within 3 percent of) twice those for the departures from the January mean in all cases.

B. DEPENDENCE ON BALLISTIC COEFFICIENT

The inverse dependence of impact displacement on β, as predicted by Eq. 10, is borne out by the data in Table 4. For three combinations of V_o and γ_o representing reentries from nearly minimum-energy trajectories, the miss distances from Table 3 are plotted against β in Fig. 12. The curves for miss distances due to density departures vary more nearly as the -2.0 power of β rather than the -1.0 from the approximate Eq. 10, and the logarithmic slopes of the curves for wind departures center about a -1.5 power dependence on β.

It is to be noted in summary of Fig. 12 and Table 4 that for ballistic coefficients above 2000 lb/ft^2 the largest miss distances from the selected range of reentry parameters will be no more than a few hundred feet for the worst wind and density departures from the monthly mean. On the other hand, for ballistic coefficients of 500 lb/ft^2 and below, the miss distances can be as much as several thousand feet under the same conditions.

Another miss distance, which would not, however, naturally fall within the scope of this paper, results from an uncertainty in the value of β itself. For standard atmospheric conditions and fixed reentry conditions, a perturbation in β from the reference value produces an impact displacement which is different for each of the different reference β's and which, in fact, varies with the reentry conditions.

TABLE 4. DISPLACEMENTS OF IMPACT POINTS FROM THE JANUARY MEAN ATMOSPHERE, USING DENSITY AND WIND DIFFERENCE PROFILES REPRESENTING MAXIMUM JANUARY DEPARTURES FROM JANUARY MEAN VALUES. (Variation in miss distances with different ballistic coefficients, reentry velocities, reentry angles, and equivalent orbital inclination (i_o = 179 deg gives head wind, 89 deg gives cross wind, and 1 deg gives tail wind))

β, lb/ft^2	V_o, ft/sec	γ_o, deg	i_o, deg	$\Delta R_{x\rho}$, ft	ΔR_{xw}, ft	ΔR_{yw}, ft
550	22,500	20	179	2777	1953	
	22,500	20	89	2876	--	1860
	22,500	20	1	2992	1844	
	22,500	30	1	1018	1092	
	22,500	40	1	324	626	
	18,750	30	1	1076	1154	
	15,000	30	1	1099	1211	
	15,000	40	1	454	804	
	15,000	50	1	177	543	
1025	22,500	20	179	1316	1035	
	22,500	20	89	1387	--	999
	22,500	20	1	1472	1053	
	22,500	30	1	214	377	
	22,500	40	1	46	182	
	18,750	30	1	281	447	
	15,000	30	1	360	532	
	15,000	40	1	97	279	
	15,000	50	1	36	181	
1975	22,500	20	179	319	331	
	22,500	20	89	334	--	328
	22,500	20	1	355	355	
	22,500	30	1	55	138	
	22,500	40	1	17	78	
	18,750	30	1	73	160	
	15,000	30	1	95	189	
	15,000	40	1	31	113	
	15,000	50	1	13	78	

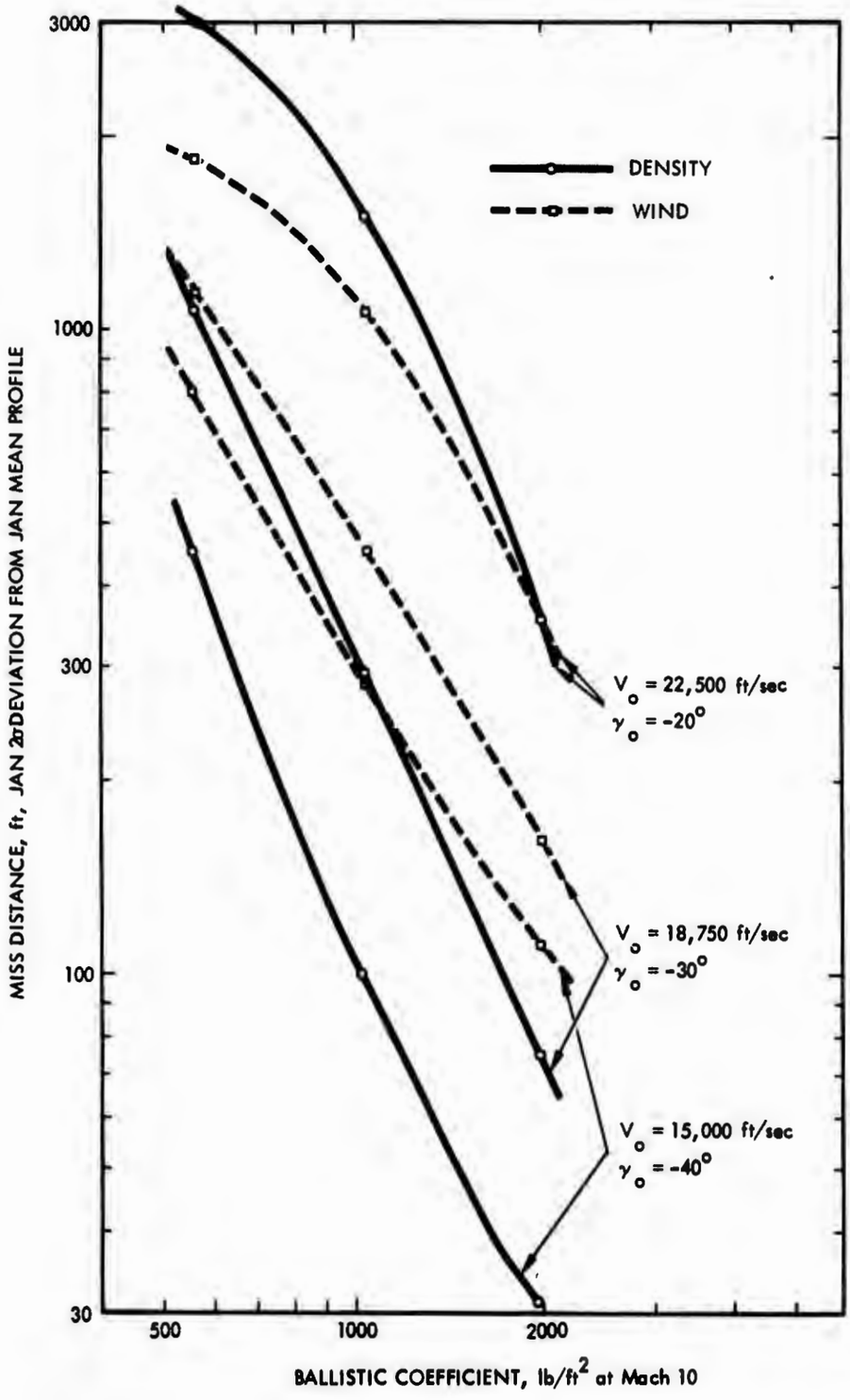

FIGURE 12. Dependence of Miss Distance on Ballistic Coefficient for Three Reentry Velocities with Nearly Minimum-Energy Reentry Angles

A 3 percent reduction in β produces the miss distances plotted for different reference β's in Fig. 13 for the same three nearly-minimum-energy reentry conditions as Fig. 12. The miss distances have nearly the same dependences on β, V_o, and γ_o as those for the worst density departure from the monthly mean in Fig. 12; the same general summary comments can be applied. A check of the linearity of the miss distance with the change in β using 2 and 4 percent perturbations indicated that the results were linear within 7 percent for β = 1975, within 2.5 percent for β = 1075, and within 1.5 percent for β = 550 lb/ft^2.

C. DEPENDENCES ON REENTRY VELOCITY AND PATH ANGLE

The miss distances from the parameter study (Table 4) are plotted as a function of reentry velocity for a 30 deg reentry angle in Fig. 14 and as a function of reentry angle for 15,000 and 22,500 ft/sec reentry velocities in Fig. 15.

The miss distance varies approximately as the -1 power of reentry velocity, in agreement with the approximate Eq. 10; the slope is slightly shallower for lower β and for the wind effects in comparison with the density effects.

The inverse variation of miss distance with $\sin^2\gamma_o$ predicted by Eq. 10 is again, as with β, short of the actual behavior. The exponent for the wind effects is more nearly 3 and for the density effects as high as 5. Lower β's show slightly lower slopes.

D. DEPENDENCE ON FLIGHT AZIMUTH

The values of the reentry velocity and reentry flight path angle are defined in the frame of reference rotating with the earth. Vehicles reentering due eastward or due westward at the equator at the same reentry velocity and path angle will have velocities in a nonrotating inertial frame which are different by twice the velocity due to the earth's rotation. The inclusion in the parameter study of equivalent orbital inclinations of 1 deg, 89 deg, and 179 deg was intended to provide evaluation of, first, the effects of the difference in inertial velocity on the response of the reentry vehicle to atmospheric density perturbations and, second, the difference in response of the reentry

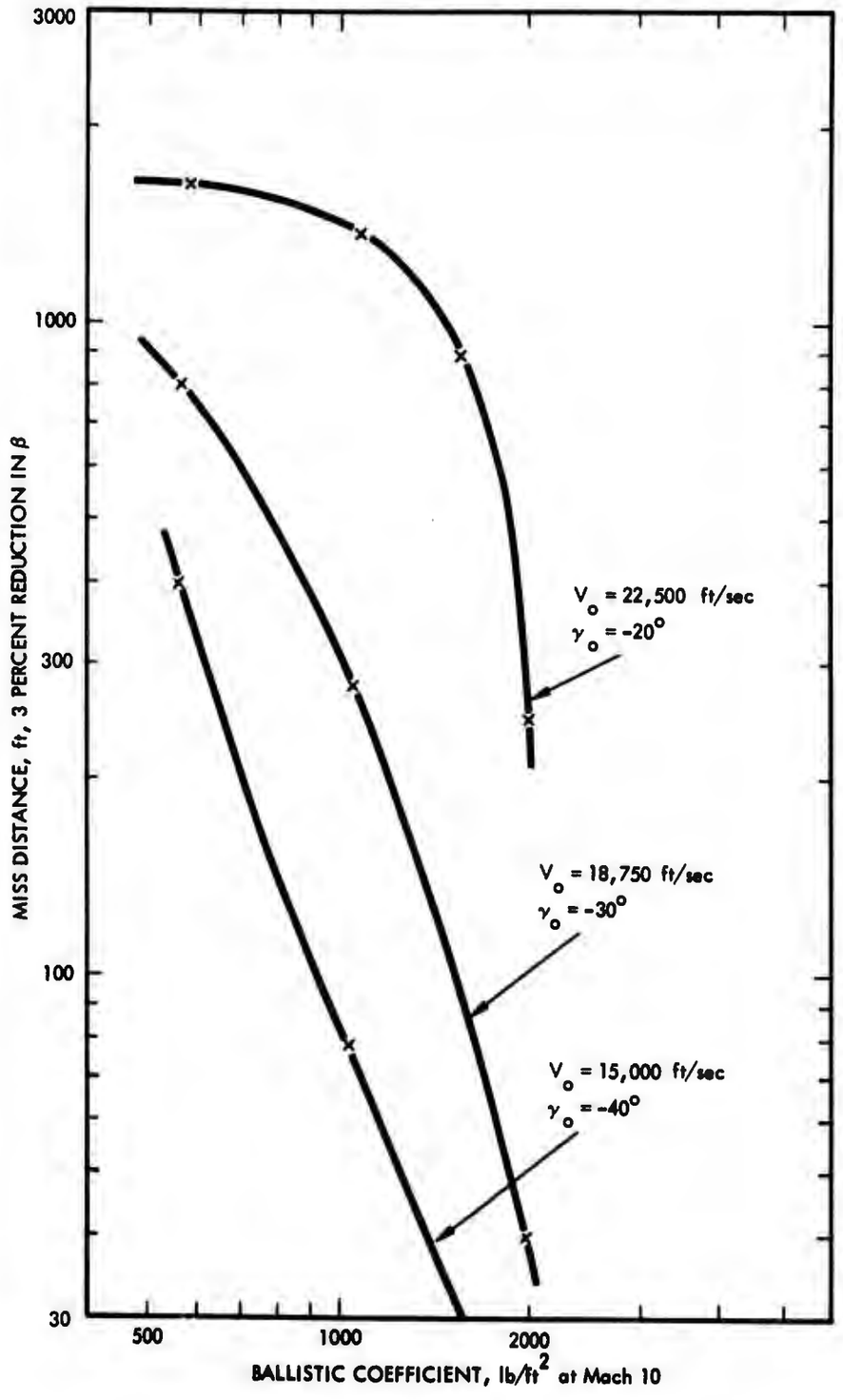

FIGURE 13. Miss Distance Due to 3 Percent Error in Ballistic Coefficient for Three Reentry Velocities with Nearly Minimum-Energy Reentry Angles

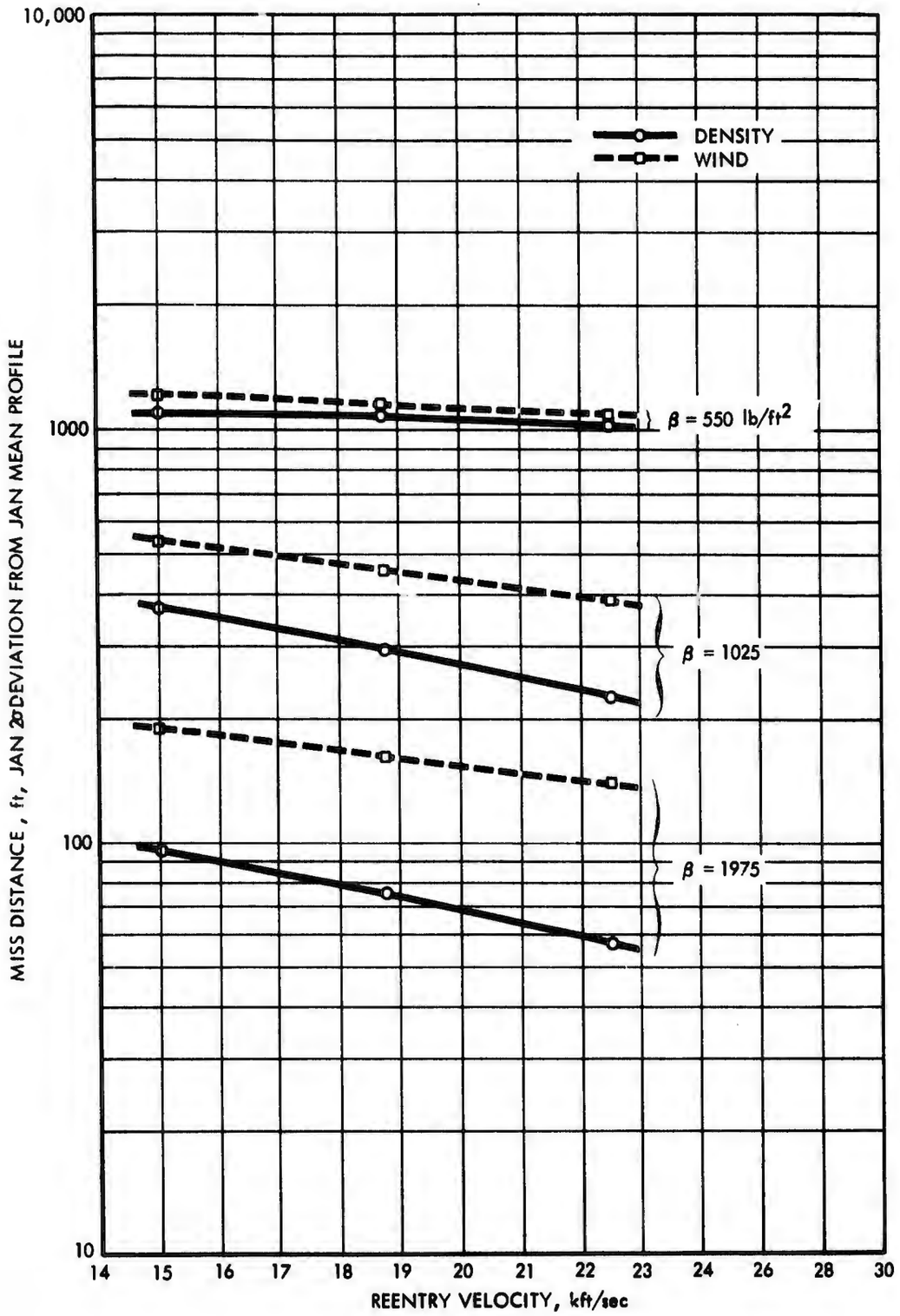

FIGURE 14. Dependence of Miss Distance on Reentry Velocity for Three β's at a Reentry Angle of 30 Deg

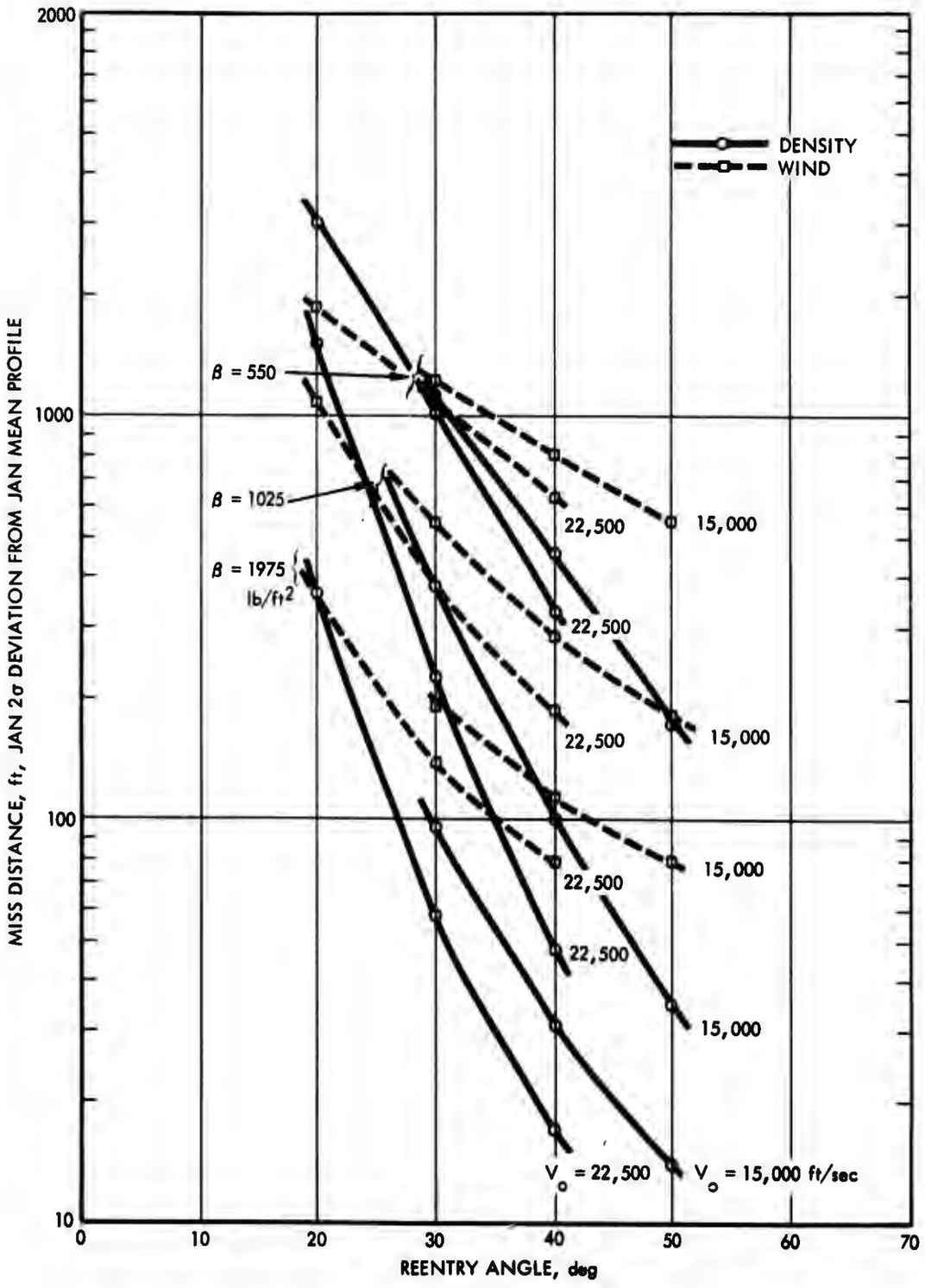

FIGURE 15. Dependence of Miss Distance on Reentry Angle for Three β's and Two Reentry Velocities

vehicle to tail winds (i_o = 1 deg), cross winds (89 deg), and head winds (179 deg). While the wind-direction effect is not really separated from the inertial velocity effects for the second comparison, the differences are felt to be indicative if not descriptive.

Inspection of the miss distances for i_o = 1, 89, and 179 deg in Table 4 shows that the density effect increases linearly with decreasing i_o, i.e., with increasing inertial velocity and decreasing inertial flight path angle. The miss distance due to density departures changes by 12 percent or less over the full range of orbital inclinations (flight azimuths) for the three β's for the 22,500 ft/sec, 20 deg reentry.

The miss distance due to westerly winds does not behave as simply. The increasing trend with decreasing i_o, like that above, for the extreme values reverses itself for the lowest β, and the miss distance for cross winds tends to be the lowest (8 percent or less below the highest) except for the β = 550 lb/ft^2 case where the tail wind gives the lowest miss distance by a fraction of a percentage point.

Flight azimuths of interest cover only a small part (less than one third) of the total possible range of values, and the maximum difference in miss distance over the total range is small (8 to 12 percent). One could, therefore, expect miss distances for interesting flight azimuths to differ by no more than a few percent, a small enough trend to be neglected in the rest of the discussion in this paper.

V. ALLOWABLE ERRORS IN MEASUREMENT OF ATMOSPHERIC PROFILES

An uncertainty in measurement of the density or wind velocity at a certain level in the atmosphere can be directly associated with an uncertainty in impact point for a reentry vehicle with specified reentry conditions. The impact error is given by multiplying the measurement uncertainty by the influence coefficient at that altitude, i.e., by the impact displacement per unit change in density or wind velocity, plotted in Fig. 11, for that level for the given reentry vehicle and reentry conditions.

With a view toward reducing impact errors due to atmospheric uncertainties, a limit can be set on the miss contribution from each individual layer, and the associated allowable measurement error can be derived from this limiting miss contribution by dividing by the influence coefficient. The resulting altitude dependence of allowable measurement errors will, therefore, be the inverse of the plots in Fig. 11, showing the smallest allowable error at that intermediate altitude where the largest miss contribution from a constant perturbation was found.

A limiting total miss distance due to atmospheric measurement uncertainties is chosen here arbitrarily as 200 ft from either wind or density independently, as a reference point from which values for other miss distances can be readily scaled.

The allowable atmospheric measurement error in each layer is defined to produce an equal fraction of the 200-ft total from all levels except for those very high-altitude (and sometimes very low-altitude) layers whose influence is so small that equal-contribution allowable errors would have exceeded 50 percent in density or 500 ft/sec in wind velocity. In those, the contribution to the 200-ft miss is limited to

that smaller value which is produced by a constant 50 percent density error or a constant 500 ft/sec wind velocity error. The sum of the constant-atmospheric-error layers' miss contributions is then subtracted from 200 ft and the remainder is divided equally among the remaining, more influential layers.

For measurement of the atmospheric properties at all levels with the same instrument, which would have a systematic error of the same sign at all altitudes, the allowable errors are calculated assuming a linear combination (i.e., a direct sum of absolute values) of the individual miss contributions. For measurement at each level with a different instrument, which would have a random occurrence of the sign of the error, the allowable errors are based on a root-sum-square combination of the miss contributions. In the linear case, the individual allowable error is essentially the total divided by the number of levels, whereas in the root-sum-square case the individual error is the total divided by the square root of the number of levels. Hence, allowable errors with a common instrument will be considerably smaller than with independent instruments at each level. An actual situation will be somewhere between these extremes; several instruments will be used to measure several layers each.

The procedures above are applied to the data of Fig. 11 and the curves of allowable density measurement error and allowable wind velocity measurement error in Fig. 16 are generated. Minimum measurement uncertainty required to limit total impact uncertainty to 200 ft, occurring at 5- to 10-km altitudes, varies from about 0.1 percent and 1 ft/sec for low β, low reentry angle and systematic error, to more than 50 percent and 200 ft/sec for high β, high reentry angle, and random error.

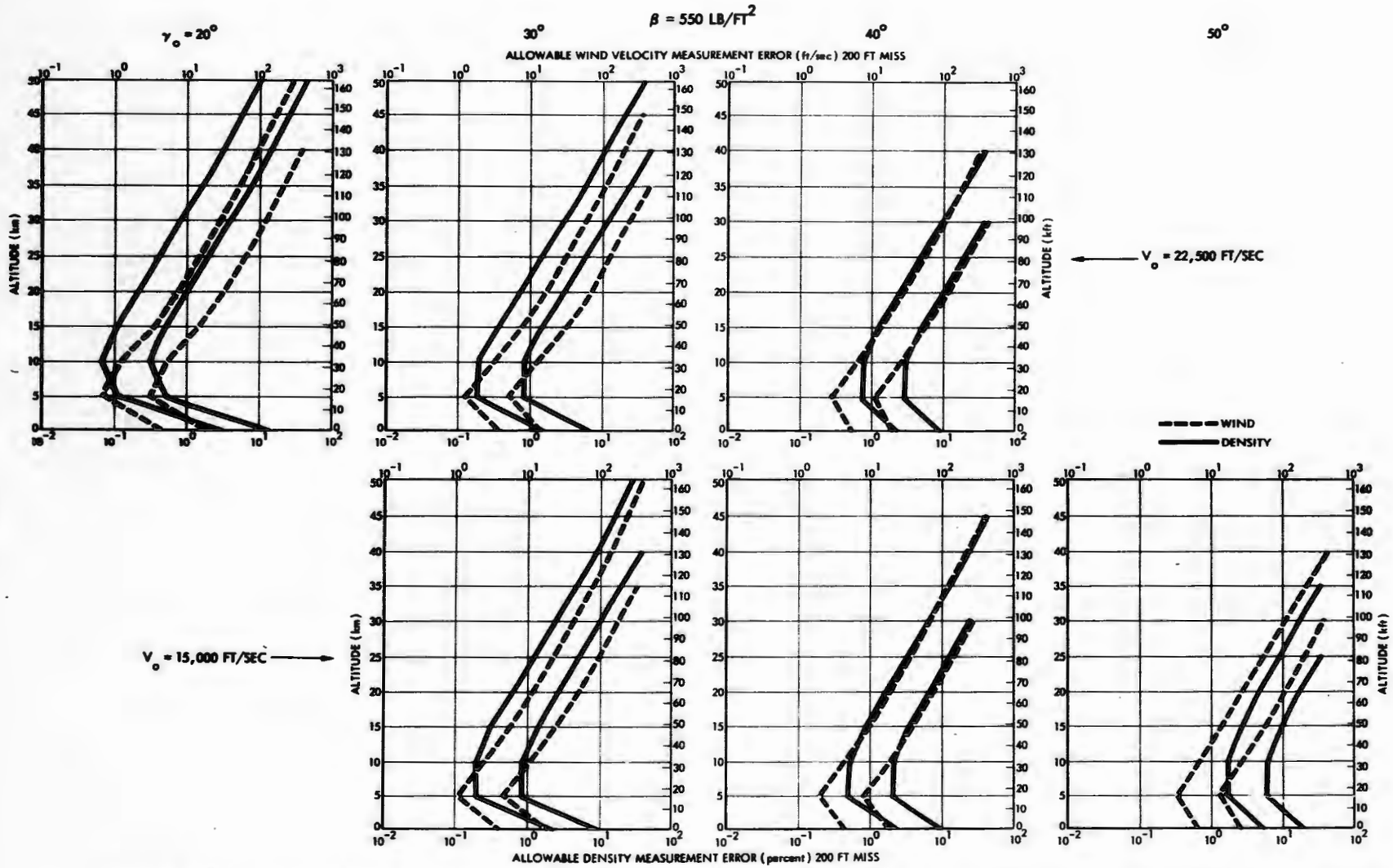

FIGURE 16a. Allowable Errors in Measurement of Atmospheric Properties at Each 5 km Altitude Level to Limit Total Miss Distance to 200 ft for Reentry Vehicle with $W/C_D A$ of 550 lb/ft^2 for Different Reentry Angles and Reentry Velocities. Right Curves Show Allowable Errors if Combined as Measurements with Different Instruments at Each Altitude Level; Left Curves Show Allowable Errors if Properties at All Levels are Measured with Same Instrument.

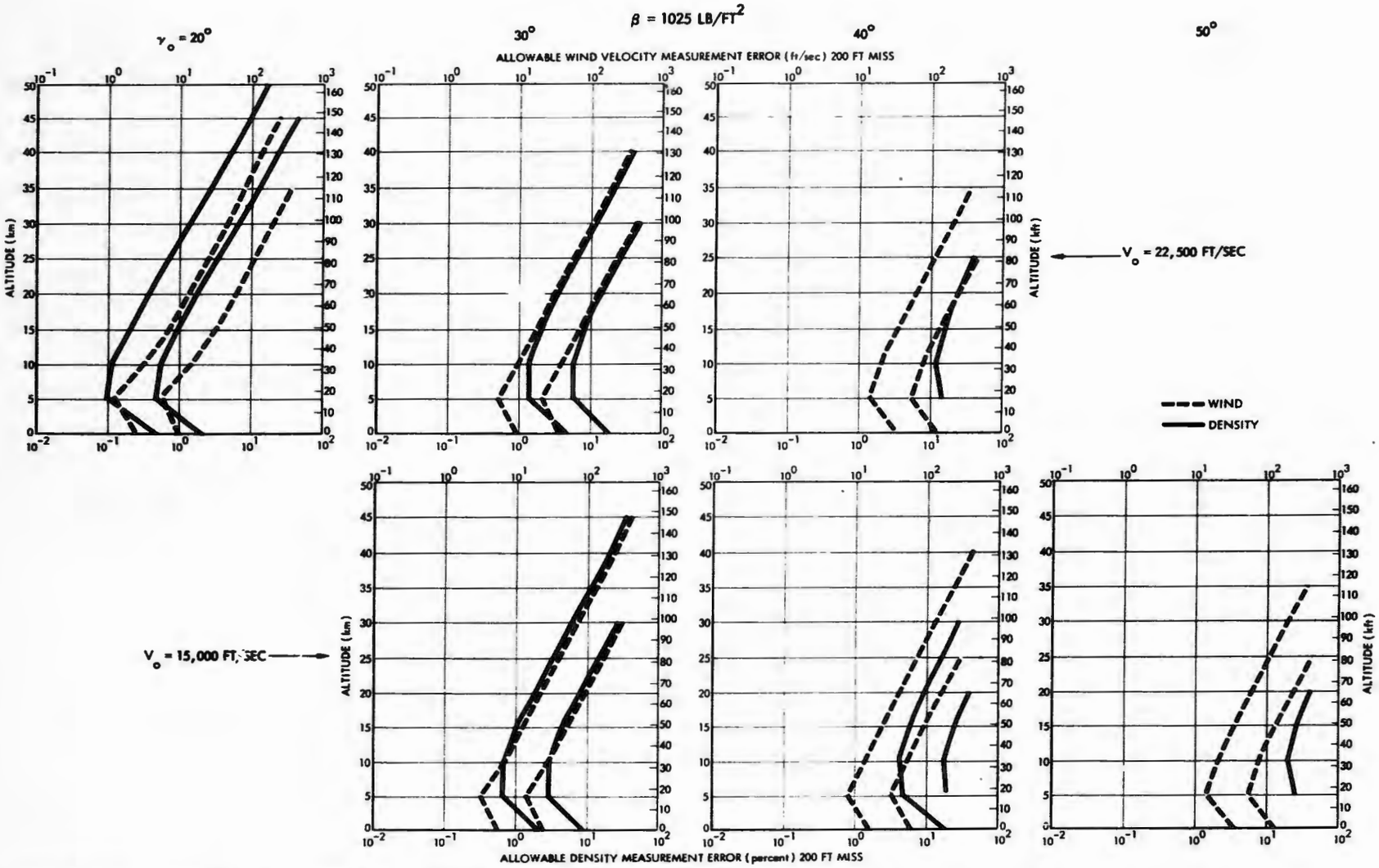

FIGURE 16b. Allowable Errors in Measurement of Atmospheric Properties at Each 5 km Altitude Level to Limit Total Miss Distance to 200 ft for Reentry Vehicle with W/C_DA of 1025 lb/ft^2 for Different Reentry Angles and Reentry Velocities. Right Curves Show Allowable Errors if Combined as Measurements with Different Instruments at Each Altitude Level; Left Curves Show Allowable Errors if Properties at All Levels are Measured with Same Instrument.

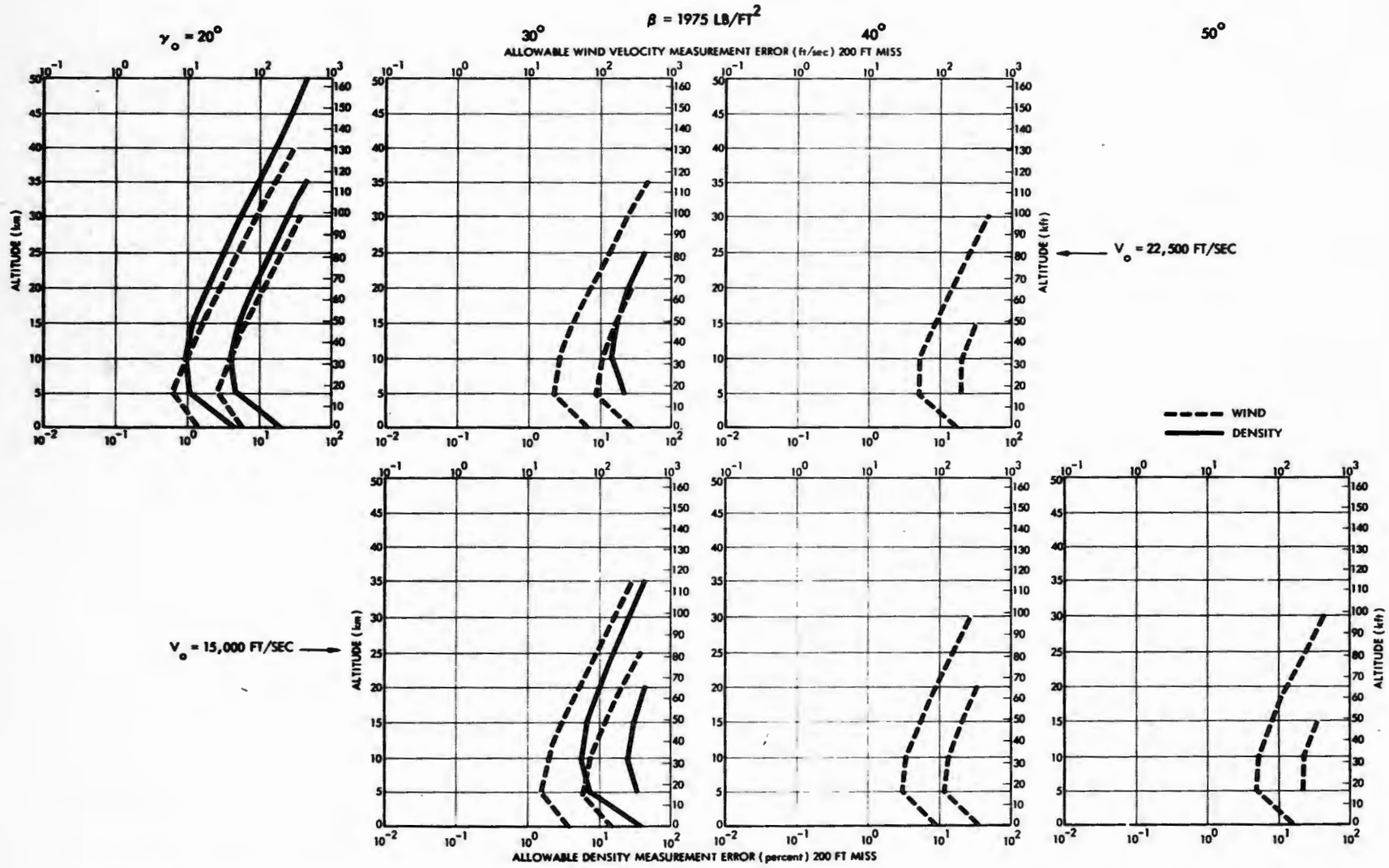

FIGURE 16c. Allowable Errors in Measurement of Atmospheric Properties at Each 5 km Altitude Level to Limit Total Miss Distance to 200 ft for Reentry Vehicle with W/C_DA of 1975 lb/ft^2 for Different Reentry Angles and Reentry Velocities. Right Curves Show Allowable Errors if Combined as Measurements with Different Instruments at Each Altitude Level; Left Curves Show Allowable Errors if Properties at All Levels are Measured with Same Instrument.

BIBLIOGRAPHY

Albini, F. A. and L. Glover, "Reentry Dispersion Calculations" (U), Appendix E to IDA Study S-242, "An Investigation of the Limits of Ballistic Missile Accuracy" (U), June 1966 (S-RD)

CIRA (1965), COSPAR International Reference Atmosphere, North Holland Publishing Company, Amsterdam.

Finke, R. G., "The RANGE Computer Code--A Multipurpose Trajectory Calculation," IDA Memorandum 27 August 1963 (U).

Kochanski, A. (1964), "Atmospheric Motions from Sodium Cloud Drifts," JGR, Vol. 69, p. 3651.

NavWeps Report 1428 (Vol. 3): "Handbook of Supersonic Aerodynamics," Section 8: "Bodies of Revolution," October 1961, (U), p. 237.

U. S. Standard Atmosphere Supplements, 1966, Environmental Science Services Administration, National Aeronautics and Space Administration, USAF.

Valley, S. L., ed., Handbook of Geophysics and Space Environments, AFCRL, and Office of Aerospace Research, USAF, pp. 9-2 to 9-14, 1965.

UNCLASSIFIED

Security Classification

DOCUMENT CONTROL DATA - R & D

(Security classification of title, body of abstract and indexing annotation must be entered when the overall report is classified)

1. ORIGINATING ACTIVITY (Corporate author) Institute for Defense Analyses	2a. REPORT SECURITY CLASSIFICATION UNCLASSIFIED 2b. GROUP --

3. REPORT TITLE

Reentry Vehicle Dispersion due to Atmospheric Variations

4. DESCRIPTIVE NOTES (Type of report and inclusive dates)
Research Paper P-506, August 1969

5. AUTHOR(S) (First name, middle initial, last name)

Reinald G. Finke

6. REPORT DATE August 1969	7a. TOTAL NO. OF PAGES 42	7b. NO. OF REFS --
8a. CONTRACT OR GRANT NO. DAHC15 67 C 0011 b. PROJECT NO. Task T-58 c. d.	9a. ORIGINATOR'S REPORT NUMBER(S) P-506 9b. OTHER REPORT NO(S) (Any other numbers that may be assigned this report) None	

10. DISTRIBUTION STATEMENT

This document has been approved for public release and sale; its distribution is unlimited.

11. SUPPLEMENTARY NOTES N/A	12. SPONSORING MILITARY ACTIVITY Advanced Research Projects Agency Washington, D. C.

13. ABSTRACT

Reentry vehicle impact displacements due to a fixed perturbation in density or in wind speed in each 5-km-thick layer of the atmosphere up to 90-km altitude have been derived from a series of machine reentry-trajectory calculations with the IDA Program RANGE for different R/V's and reentry conditions. Three arbitrary reentry vehicle shapes were chosen whose ballistic coefficients (550, 1025, and 1975 lb/ft^2) were representative of the range of interesting values. Reentry conditions were varied, from those of IRBM's of 15,000 ft/sec at 50-deg path angle, to those for ICBM's of 22,500 ft/sec at 20-deg path angle, and reentry azimuths were varied from direct equatorial (tail wind) to retrograde equatorial (head wind). Intermediate reentry conditions were included to define the dependences well enough for interpolation, and even slight extrapolation, to all known interesting combinations.

The resulting layer-wise miss contributions from the most influential 5-km layers (centered at 5- and 10-km altitude) vary from about 200 ft for 1 percent change in density, or about 20 ft for 1 ft/sec change in wind speed for the low β and low reentry angle, to 0.4 ft for either 1 percent density change or 1 ft/sec of wind for the high β and high reentry angle.

At 60° N latitude, the worst case, ~2σ density and wind departures from a monthly mean profile occur in January and amount to about 5 percent in density and 50 ft/sec in wind in the most influential 5- to 10-km-altitude range. The corresponding total miss distances due to the combined departures from the mean profile for all altitudes range from several thousand feet for the low β, low reentry angle down to several tens of feet for the high β, high reentry angle. These total miss distances vary as the minus 1.5 to 2 power of β, as the minus 1 power of reentry velocity, as the minus 3 to 5 power of the sine of the reentry angle, and negligibly with flight azimuth.

Allowable measurement errors for each layer to give a total impact uncertainty of 200 ft from combinations of all layers were derived. The minimum allowable errors in density and wind, occurring of course in the most influential 5- to 10-km layers, increase from the tightest extreme of about 0.1 percent and 1 ft/sec for low β, low reentry angle and combination as with common systematic error, to more than 50 percent and 200 ft/sec for high β, high reentry angle and combination as with random error.

DD FORM 1 NOV 68 1473

UNCLASSIFIED

Security Classification

DISTRIBUTION LIST FOR RESEARCH PAPER P-506

ODDR&E

Dr. John S. Foster, Jr. (Director, ODDR&E)
Dr. Roland F. Herbst (Dep. Director, Strat. & Space Sys.)
Mr. C. Robert Wieser (Asst. Director, Defensive Weapons)
Dr. Ronald L. Easley (Asst. Dir., Strat. Sys. Rev. & Anal.)
Mr. Ben T. Plymale (Asst. Director, Strategic Weapons)
Mr. Walter McGough (Spec. Asst., Threat Assessment)
Mr. George R. Barse
Mr. Clifford McLain

ARPA

Dr. Eberhardt Rechtin, Director
Dr. S.J. Lukasik, Deputy Director
Dr. David E. Mann, Strategic Technology
Major J.L. Torres, USAF, STO
Dr. J.P. Wade, Jr., STO
Mr. Fred A. Koether, TIO

Department of the Air Force

Headquarters, SAC
Offutt Air Force Base, Nebraska 68113
1. DCS/Operations
2. DCS/Intelligence
3. Ballistic Missile Evaluation Agency (Col. Slagle)
4. JSTPS
5. Operations Analysis (B.F. Stafford)

1st Strategic Aerospace Division
Vandenberg Air Force Base, Calif. 9343?

Headquarters, USAF
Washington, D.C. 20330
1. AFNINE
2. AFRDDF
3. AFRDQSS2
4. AFRDSA
5. AFRDSC
6. AFRDS (CCG-QMS)
7. AFRDSD
8. AFXOSS

L.G. Hanscom Field
Bedford, Mass. 01730
1. AFCRL (CRT)
2. AFCRL (CRH)
3. Dr. K.S.W. Champion (CRUB)

Headquarters, AFSC
Andrews Air Force Base,
Washington, D.C. 20331
1. SCSS
2. SCW

6th Weather Wing (6 VS)
Andrews Air Force Base
Washington, D.C.

Headquarters, Air Weather Service
Scott Air Force Base, Illinois 62225
1. Dr. Fletcher (AWVDC)
2. Col. Best (AWODC)

Headquarters, Office of Aerospace Research
1400 Wilson Blvd.
Arlington, Va. 22209
1. Mr. Gallie (RRO)
2. Col. Downie (RRY)

Air Force Office of Scientific Research
1400 Wilson Blvd.
Arlington, Va. 22209
1. Dr. Price (SRG)
2. Mr. Best (SRP)

Space and Missile Systems Organization
Air Force Unit Post Office
Los Angeles, Calif. 90045
Attn: Brig. Gen. Robert Duffy (SMY)
Col. Botzong (SMUH)
Col. Paul Osborn

Department of the Army

Office of the Chief of Research and Development
The Department of the Army
Washington, D.C. 20310
1. Dr. Halley, Science Advisor,
Director of Missiles & Space
2. Lt. Col. Lombard, Space Branch, CRDMS
3. Mrs. Whedon, CRDES

Mr. Murray Miller
U.S. Army Satellite Communications Agency
Fort Monmouth, N.J. 07703

Commanding Officer, ASL
Fort Monmouth, N.J. 07703

Mr. Talley
Headquarters, CDC
Fort Belvoir, Va. 22060
Attn: CDCMR-E

Commanding Officer, CDC FA Agency
Fort Sill, Okla. 73503

Commanding Officer, CDC ADA Agency
Fort Bliss, Texas 79916

Department of the Navy

Commanding Officer
Naval Weather Research Facility
Naval Air Station
Norfolk, Va. 23511

Commanding Officer
Fleet Weather Central
Naval Air Station
Norfolk, Va. 23511

Commanding Officer
Fleet Numerical Weather Central
Naval Post Graduate School
Monterey, Calif. 93940

Commanding Officer
U.S. Fleet Weather Central
Box 12, COMNAVMARIANAS
P.O. San Francisco 96630

Commanding Officer
Fleet Weather Central
Box 113, FPO San Francisco 96610

Commanding Officer
U.S. Fleet Weather Central
Box 31, FPO New York 09540

Naval Research Laboratory
Washington, D.C. 20390
1. Dr. William R. Faust (Code 5100)
2. Mr. Roger L. Easton (Code 5160)

Commanding Officer
U.S. Naval Weapons Laboratory
Astronautics Division
Dahlgren, Va. 22448
1. Code KA
2. Code KR

Commanding Officer
U.S. Naval Weapons Laboratory
Code ATT KXR
Dahlgren, Va. 22448
Attn: Mr. Fenn
Mr. David Brown

Officer in Charge/NASE
Project FAMOS
U.S. Fleet Weather Central
Department of the Navy
Washington, D.C. 20390

Miscellaneous Government

Defense Intelligence Agency
Washington, D.C.
Attn: DIAST 3B
Mr. A.J. Murri

Commander, Joint Meteorological Satellite
Project Office
1400 Wilson Boulevard
Architect Bldg., Rm. 742
Arlington, Va.
Attn: Col. A. Kouts

Industry

Aerospace Corporation
P.O. Box 5866
San Bernandino, Calif. 92408
Attn: Dr. N. Nichols
Dr. F. Fernandez
Dr. Allen Schaeffer

Applied Physics Laboratory
Silver Spring, Maryland
Attn: Mr. Louis Glover

Rand Corporation
1700 Main Street
Santa Monica, California
Attn: Dr. Albert Latter

TRW Corporation
One Space Park
Redondo Beach, Calif.
Attn: Mr. Dan Scalley
Mr. Don Piehler

Environmental Technical Applications Center
Suitland, Maryland
Attn: Major G.R. Farr

Universities

Professor G.J.F. MacDonald
Vice Chancellor for Research and Graduate Affairs
University of California
Santa Barbara, Calif. 93106

Professor V.E. Suomi
University of Wisconsin
Madison, Wisconsin

Stanford University
Dept. of Aeronautics and Astronautics
Palo Alto, California
Attn: Professor Robert Cannon

Defense Documentation Center (50)
Cameron Station
Alexandria, Virginia

IDA

Mr. J. S. Attinello
Mr. J. J. Bagnall
Mr. A. R. Barbeau
Dr. M. D. Barnett
Dr. E. Bauer
Dr. V. J. Berinati
Mr. P. Cutchis
Dr. A. H. Flax
Dr. R. H. Fox
Mr. G. Gordon
Dr. A. J. Grobecker
Mr. H. Hidalgo
Dr. J. A. Laurmann
Mr. C. S. Lerch, Jr.

Dr. G. A. Massell
Mr. L. P. Minichiello
Dr. R. C. Molander
Mr. J. C. Nolen
Dr. R. C. Oliver
Dr. B. Paiewonsky
Dr. R. E. Reichenbach
Dr. W. J. Schultis
Dr. T. E. Sterne
Mr. A. J. Tachmindji
Dr. B. L. Tucker
Mr. W. A. Van Zeeland
Mr. M. C. Vosburgh
Dr. M. Watter
Mr. E. T. Williams
Dr. H. G. Wolfhard